Westinghouse Research Laboratories

DISCLAIMER NOTICE

THIS DOCUMENT IS THE BEST QUALITY AVAILABLE.

COPY FURNISHED CONTAINED A SIGNIFICANT NUMBER OF PAGES WHICH DO NOT REPRODUCE LEGIBLY.

Proprietary Class 1

Strictly limited. Cannot under any circumstances be distributed outside the Company. Inside the Company, recipient must have a specific need for the information in the conduct of his assigned responsibilities.

Proprietary Class 2

Distribution only within the Company. Copies of such documents cannot be either given or shown to anyone outside the Corporation except (1) licensees (with Associated Companies' approval) and (2) the government in proposals for contracts.

Proprietary Class 3

Unlimited distribution, both inside and outside the Company.

Westinghouse Research Laboratories Pittsburgh 35, Pa.

SEMI-ANNUAL TECHNICAL REPORT

TRANSPORT STUDIES OF DEFECT STRUCTURE INORGANIC COMPOUNDS

APRIL 1, 1964 through
SEPTEMBER 30, 1964

WESTINGHOUSE RESEARCH LABORATORIES PITTSBURGH 35, PA.

TRANSPORT STUDIES OF DEFECT STRUCTURE OXIDES

Reference: Contract Nonr-3800(00)
Authority NR359-444
ARPA Order No. 300, A. #3,
Program Code No. 4980
Semi-Annual Technical Report,
1 April 1964 thru 30 Sept. 1964
Transport Studies of Defect
Structure Inorganic Compounds
Period of Performance:
1 April 1964 thru 31 March 1965
Amount: $245,282.00
Project Scientist: R.R. Heikes,
Telephone 412-242-1500
Ext. 682-683

Table of Contents

THE EFFECT OF ELECTRODE PRETREATMENT ON THE OXYGEN REDUCTION ON PLATINUM IN PERCHLORIC ACID

Y. L. Sandler
E. A. Pantier

Abstract

The effect of pretreatment of a platinum electrode on the electrochemical reduction of oxygen and of hydrogen peroxide in perchloric acid was studied at room temperature. Hydrogen and oxygen pretreatments affect the oxygen reduction in a manner similar to cathodic and anodic pretreatments, respectively. Removal of strongly bound oxygen by hydrogen pretreatment or cathodization accelerates the decomposition of hydrogen peroxide and increases the open circuit potential and the rate of the oxygen reduction in solutions containing 10^{-5} to 10^{-7} M peroxide. Decay rates from a high anodic potential provide a sensitive measure for peroxide concentrations in the electrolyte.

One of the main difficulties in studying the electrochemical oxygen reduction reaction on platinum in acid solution is the lack of reproducibility under varying conditions. This is due to differences in impurity content, the peroxide concentration of the solution and the physical characteristics of the electrode. This report mainly deals with the influence of the latter on the characteristics of the electrode reaction.

Hydrogen peroxide is either an intermediate[1] or a by-product[2,3] in the reduction reaction of oxygen. In practice, therefore, it is always present when a cathodic current is drawn as, for example, in fuel cells.

In clean solutions and at very low peroxide concentrations, open circuit potentials (OCP) of close to 1.23 volts versus a hydrogen electrode in the same medium have been obtained in the past by special pretreatments.[2,3,4] The potentials were assumed to be true reversible potentials, corresponding to a four-electron reduction of oxygen to water. The potential cannot be reproduced after a cathodic current is drawn.

At high peroxide concentrations, above 10^{-4} mole per liter, a potential of about 0.84 volt[5] is set up which is characteristic of the peroxide electrode and independent of the ambient atmosphere and the peroxide concentration. For the oxygen reduction reaction OCP's usually lie between 0.8 and 1.1 volt. The oxygen coverage is below one monolayer.[6]

In a previous study[7] of the oxygen adsorption on platinum and silver in a dry system, different types of chemisorptions were found varying in binding energy. The activity of the surface for the reaction

$O^{16}_2 + O^{18}_2 \rightarrow 2\ O^{16}\ O^{18}$ was found to be affected by the presence of firmly bound oxygen adsorbed at high temperatures, and by the presence of hydrogen in the surface.

In the present study the effect of the high temperature pretreatment of the platinum electrode with oxygen and with hydrogen on the characteristics of the oxygen electrode in perchloric acid solutions was studied. A reproducible effect of gas pretreatment was found and was compared with the effect of electrochemical prehistory. This method of comparison was used to study the influence of the nature of the adsorbed oxygen on the electrochemical characteristics of the electrode.

EXPERIMENTAL

The Cell: The cell consisted of a flanged 5 inch diameter Pyrex vessel closed by a lid and a teflon gasket. The electrodes were introduced through the lid via ground joints fitted with teflon sleeves. The counter-electrode tube and the Luggin capillary tube contained fritted glass discs separating the corresponding electrodes from the main body which contained the test electrode and the oxygen bubbler. A platinized platinum coil served as hydrogen electrode which was frequently checked against a second hydrogen electrode.

Gases: Commercial electrolytic oxygen was purified by passage through hot copper, Dryerite, Ascarite, and a molecular sieve at dry ice temperature. Hydrogen was also an electrolytically produced commercial

product. It was passed over hot palladium asbestos, Dryerite and molecular sieve at liquid nitrogen temperature.

The Electrolyte: Reagent grade perchloric acid was used. It was diluted with water distilled from alkaline permanganate and then double distilled in a quartz still.

The Electrodes: Platinum foils of 99.999% purity were used in form of a square, one-half inch each side. After degreasing in hot 20% KOH, the foils were treated in hot 50% nitric acid and carefully washed in triple distilled water and in condensing steam.

Heat Pretreatment: The foils having platinum lead wires spot-welded to them were cleaned, mounted in their quartz electrode holders and fitted into a quartz furnace tube. The foils were treated in a flow of oxygen at increasing temperature with at least two hours at 700°C. The tubes were then plugged and transferred to a glove box flushed with pure oxygen. Inside the box the electrode holder and foil were transferred to the cell.

In the case of "hydrogen pretreated foils" the same procedure was adopted except that after the oxygen treatment at 700°C the oxygen was displaced by helium and the foil was treated for two hours with hydrogen at 600°C. The foils were then cooled in helium and again exposed to oxygen at a temperature below 100°C for at least one-half hour. Oxygen was bubbled over the electrode, except where stated otherwise.

Instrumentation: Potentials were read with a Keithley model 660 differential voltmeter. Open circuit potentials were read at infinite input impedance using the Kelvin-Varley divider on the instrument. A Varian recorder was only used when the lower input impedance of the direct reading device (about 10^7 ohm) was considered not disturbing. Approximately constant currents were obtained by means of mercury batteries giving 28 volts and a set of fixed and variable resistors in series with the cell. Currents were measured by means of a Keithley electrometer, model 200B, and current shunt.

RESULTS

The Reduction of Oxygen:

The following experiments are examples of the effect of the electrochemical pretreatment of solution and electrode on the current-voltage characteristics. The measurements shown in Fig. 1 were carried out in 1/10 N perchloric acid which was pre-electrolyzed for 60 hours at 10 mA with oxygen bubbling through it. Two platinum pre-electrolysis electrodes of about 1 cm^2 area were in the main compartment of the cell which was later occupied by the test electrode. This type of pretreatment purifies the solution but generates hydrogen peroxide. The test electrode was dipped for 20 minutes in hot 50 % nitric acid, washed and steamed before use, but was not treated thermally. The open circuit potential, versus hydrogen in the same medium, varied from 0.80 volts at a high oxygen bubble rate to .88 volt when the oxygen was shut off. The rise in

potential, described in literature,[8] is due to the catalytic destruction of the peroxide at the electrode as will be discussed later on. The points shown in all figures were taken after 4 minutes at constant current. Only the open circuit potentials (OCP) will be given as obtained 30 to 60 minutes after immersing the electrode or interrupting the current.

Curve 1 gives the cathodic galvanostatic polarization curve for increasing current settings. An overshoot at first occurred with each new current setting increasing to 25 mV at 10^{-3} Amp. The potential then rose and became stationary within the given time. Currents were always cut off when strong fluctuations started indicating approach of the limiting current before drop to low potentials in the hydrogen evolution region. On decreasing the current a stronger overshoot occurred. The overshoot with increasing cathodic polarization is believed to be due to removal, or increasing the current, of strongly bound oxygen which decreases the activity of the electrode, as discussed later. On decreasing the polarization the reverse process occurs.

After leaving the current at 1×10^{-4} overnight, the OCP was higher, having risen to 0.962 Volt. Another cathodic sweep then taken is shown in Fig. 1, curve 2. While the polarization was now lower at low currents it was higher at high currents. No good Tafel region was found; the approximate slope was 160 mV between 10^{-5} and 5×10^{-4} Amp, while it was 115 mV in curve 1. The overshoot on the return curve as a function of time is indicated in Fig. 1 by the points at 4×10^{-4} and 1.3×10^{-5} Amp.

After anodizing the foil several times in the same solution to about 1.8 Volt (to determine the decay rate, as described below) the open circuit voltage was found to be low, viz. 0.835 Volt. A cathodic curve then taken is shown as curve 3 in Fig. 1. The potential was now relatively low at low currents and high at high currents. The described behavior was qualitatively well reproducible: cathodizing at high current gave a relatively high open current potential and a steep slope while anodizing gave a low potential at open circuit but a small decrease in potential with increasing current.

The rate of decay measured after charging the foil anodically to 1.8 Volt was measured oscillographically; it indicated peroxide concentration of the order of 10^{-4} mole/liter (see below).

In Fig. 2 curves obtained after different gas pretreatments of the electrode are presented. Curve 1 was obtained after the hydrogen pretreatment described in the Experimental Section. The initial open circuit potential was 0.97 Volt. On the following day the OCP was 0.94 Volt. A cathodic sweep for increasing and decreasing current was taken which is shown in Fig. 2, curve Ic. The high open circuit potential and the steep slope of 160 mV are very similar to what was obtained after cathodizing in Fig. 1. After anodizing, again a low open circuit potential, .83 Volt, and a flat characteristic was obtained (not shown). Curve 2 in the same figure shows the results after thermal oxygen pretreatment of another foil in a new solution. The open circuit potential was low immediately, .85 Volt, and the slope of the cathodic curve was small. This is similar to what was previously obtained after anodizing (Fig. 1).

Several experiments were made with gas pretreated electrodes in which the solution was only anodically pre-electrolyzed[3] for 20 hours at 5 mA. In these experiments the main cell compartment, later used for the test electrode, contained an auxiliary electrode serving as an anode, while the counter electrode was used as the cathode. This resulted in a lower peroxide concentration. Figure 3 shows two sets of curves in which the anodic sweeps were taken first, in 1 N perchloric acid. The anodic potential values rose steadily and were taken after 4 minutes. It may be seen that the initial values for the hydrogen pretreated electrode are higher again, 75 mV at open circuit. In the present case this even holds for the cathodic sweeps taken after anodization although this was not always found. The potential for an electrode which was not thermally pretreated was intermediate between the values found for oxygen and for hydrogen pretreated electrodes. Similar differences were also obtained when the cathodic sweeps were taken first, giving OCP's of 1.02 and 0.94 Volt respectively. The peroxide concentration in these experiments was of the order of 10^{-7} mole/liter.

Estimation of the Peroxide Concentration:

The peroxide concentrations were estimated in two ways, (1) from the anodic limiting current, (2) from the rate of decay from a given high potential. In Fig. 3 the rate of rise to the oxygen evolution potential (1.45 Volt) became appreciable below 10^{-6} Amp/cm^2. The limiting current i_L is related to the diffusion coefficient, D, by the relation

$$i_L = \frac{2FD}{\delta} c \quad .$$

Winkelmann's[9] experimental results can be presented by the simple approximate relation

$$i_L \ (\text{Amp/cm}^2) \approx c \ (\text{mole/lit}) \quad .$$

Therefore the peroxide concentration in the present case was below 10^{-6} mole/liter.

Figure 4 shows a set of decay curves obtained with different added peroxide concentrations after charging the oxygen electrode to 1.8 volt. The decay rate may be seen to be a function of the peroxide concentration. A corrosion-like reaction apparently takes place involving the reduction of unstable surface oxygen and the simultaneous oxidation of peroxide. The approximate concentration of 10^{-7} mole/liter was found for the examples given in the previous paragraph by comparing the measured decay curves to the given set of standard curves.

In peroxide-free solutions, the decay[11] of the polarization would give a slope of only about 120 mV. The method, therefore, can be extended to even lower peroxide concentration and by far exceeds the sensitivity limit of chemical tests.

The Reduction of Peroxide:

The reduction of peroxide in 1N perchloric acid in helium-saturated solutions was also studied and compared to the oxygen reduction in the same electrolyte.

In Fig. 5, curves (a) and (b) show cathodic polarization curves at a concentration of added peroxide of 10^{-3} mole/liter, as obtained with a hydrogen pretreated electrode in helium and oxygen saturated solutions, respectively. Curves (c) and (d) were similarly obtained with a peroxide concentration of 10^{-4} mole/liter. It may be seen that the curves obtained with oxygen and with helium are practically identical up to the sharp potential drop in the helium-saturated solutions when the limiting current for the given peroxide concentration is approached at 10^{-3} and 10^{-4} amp/cm^2, respectively.

Curve (e) was obtained with an oxygen-pretreated electrode in a 10^{-4} molar helium-saturated peroxide solution. In all cases the OCP upon immersion was about 0.90 volt ($\pm$ 25 mV); for all hydrogen pretreated electrodes, it decayed to 0.85 volt within 30 minutes, while for two oxygen pretreated electrodes the OCP was only 5-10 mV lower. On the other hand, an oxygen pretreated electrode which was exposed to laboratory air for one minute gave an OCP as low as 0.80 volt.

In 10^{-5} molar peroxide solutions the oxygen reduction curve lies clearly above the peroxide reduction curve, as seen from Fig. 6. Again a hydrogen pretreated foil was used. (The cathodic limiting current was relatively high, about 10^{-4} instead of the 10^{-5} amps/cm^2 expected, presumably due to incomplete oxygen removal from the solution.)

In all cases again a distinct overshoot was found when decreasing the cathodic polarization. It amounted to between 30 and 80 mV on opening the circuit and returned to within 10 mV of the original OCP within about 30 minutes. Also a small stirring effect on the OCP was

found at all peroxide concentrations. The potential in unstirred solutions was about 15 mV higher than at high stirring rates.

Catalytic Decomposition of Peroxide by Platinum:

The higher OCP of the hydrogen pretreated or cathodized platinum electrodes at low peroxide concentrations may be explained by a higher decomposition rate of the peroxide. To test this possibility the catalytic decomposition by differently pretreated electrodes was studied.

Two electrodes which were stored after use in the preceding experiments in triple-distilled water were first used in qualitative tests. An oxygen pretreated electrode stored for one week formed practically no bubbles on the electrode surface when dipped into a 1% aqueous peroxide solution, while a hydrogen-pretreated electrode stored for two weeks rapidly covered itself with oxygen bubbles.

In a more quantitative experiment, a new platinum foil was oxygen pretreated and then dropped into a 1% peroxide solution in perchloric acid. The gas evolved was collected in an inverted burette. A gas evolution rate of 0.01 cc of oxygen per minute was measured. The rate gradually decreased to 1/3 in the course of 16 hours.

The experiment was repeated with the same foil after hydrogen pretreatment. After the usual exposure to oxygen at room temperature (see Experimental Section) the oxygen evolution rate in the solution was measured and found to be 0.10 cc per minute, i.e., 10 times larger than in the previous experiment.

DISCUSSION

As Gerischer[10] and Winkelmann[9] have shown, the catalytic decomposition of hydrogen peroxide is the result of an overall anodic process

$$H_2O_2 \rightarrow O_2 + 2H^+ + 2e^- \qquad (1)$$

and an overall cathodic process

$$H_2O_2 + 2H^+ + 2e \rightarrow 2H_2O \qquad (2)$$

proceeding at equal rates when no current is flowing. The OCP in oxygen-free stirred peroxide solutions is 0.85 volts; it is a mixed potential set up by the two given reactions.

Since the gas pretreatment did not change the peroxide potential appreciably, w conclude that the rates of the two reactions, (1) and (2), are about equally affected by the pretreatment. On the other hand, the drop in OCP, found for a poisoned electrode, is to be explained by a larger decrease in the rate of step (2). The reduction of peroxide may be expected to be more sensitive to poisoning of the metal surface because, contrary to step (1), step (2) involves the complete dissociation of an oxygen-oxygen bond.

In the oxygen reduction experiments, the peroxide concentrations in the bulk of the electrolyte were approximately constant. They, therefore, represent no steady state condition. This particularly holds for the higher peroxide concentrations and the regions of low polarization.

At low peroxide concentrations, it was found that in all cases the potential at a given oxygen reduction rate depended on the electrode pretreatment. It was lower when the electrode was thermally pretreated with oxygen at high temperature than when pretreated with hydrogen before contact with oxygen at a low temperature. Anodization or cathodization had effects qualitatively similar to the thermal pretreatment: after anodization the potential was depressed at open circuit and low cathodic polarization, while after cathodic polarization it was raised.

The dependence of the decomposition rate of hydrogen peroxide on the pretreatment suggests a simple explanation for the dependence of the open circuit potential on pretreatment found in the experiments. At relatively low peroxide concentrations (10^{-5} to 10^{-7} mole/lit) the O_2/H_2O_2 couple may mainly determine the open circuit potential, as is usually assumed for alkaline solutions.[11] At the higher potentials other equilibria such as oxygen chemisorption or metal-metal ion equilibria may also be of importance and the reduction of oxygen may be balanced by the oxidation of impurities. The standard potential of the O_2/H_2O_2 couple is 0.68 volt[12] and, according to the Nernst equation, the potential rises by $2.30 \times \frac{RT}{2F} = 30$ mV with each decade of decreasing H_2O_2 concentration. In view of the catalytic activity of the electrode no true equilibrium can exist with the bulk of the solution. The rise in OCP after hydrogen pretreatment or cathodization then is a consequence of the increased activity of the electrode which lowers the concentration of peroxide in the diffusion layer. Similarly, the dependence of the gas

flow can be explained by a change in convective transport: the concentration of peroxide at the electrode further diminishes as the flow rate decreases.

The overshoot found on changing the current may be explained by a change in catalytic activity as the oxygen content of the surface changes. Breiter,[13] from a study of periodic sweeps taken at a much faster rate, suggested that adsorbed oxygen hindered the dissolution reaction. The long lasting effects observed in our work show that these are due to oxygen strongly embedded below the outer surface. The oxygen changes the activity of the surface but does not directly enter into the reaction. The similarity of the effect on the potential of cathodic pretreatment and hydrogen pretreatment confirms this explanation. Nevertheless, the adsorption and desorption of impurity anions may have contributed to the observed effects. The dependence of the OCP on the stirring rate at high peroxide concentrations is presumably not a consequence of the catalytic decomposition of the peroxide because the mixed potential[10] would be expected to be independent of the peroxide concentration.

The effect of hydrogen pretreatment may not only be due to removal of the strongly embedded oxygen but also to hydrogen retained in subsurface solution and stabilized by the presence of oxygen. Recent experiments[7] have shown that the isotopic reaction $O^{16}_2 + O^{18}_2 \rightarrow 2\,O^{16}\,O^{18}$ is catalyzed at relatively low temperatures when platinum is pretreated with hydrogen. Similarly, experiments with silver showed that

both removal of strongly bound oxygen and the presence of hydrogen in the subsurface increase the low temperature activity for the oxygen exchange reaction but in a different manner.

A full discussion of the cathodic polarization curves is beyond the scope of this paper and would require knowledge of the intermediate steps and of the effect of the activity of the electrode on these steps. Thus, for example, the gas phase experiments[7] mentioned indicate that the rate of a possible first step in the reduction reaction $O_2 + e^- \rightarrow O_2^-$ (ads) is also dependent on the activity of the electrode. The problem is particularly complex because the oxygen coverage decreases with increasing polarization and thus the activity of the electrode changes, as is seen in the present experiments. The rate constants of some of the intermediate steps therefore change with polarization in a manner difficult to predict.

Another complication may arise in long-term polarization studies. Gas phase experiments[14] have shown that the nature of the adsorbed oxygen tends to change with time; it changes to a more stable form which decreases the catalytic activity. It thus may be expected that a slow deactivation of the platinum electrode, kept at a constant potential, would be observed even in absence of impurities.

The authors are indebted to Dr. T. Hurlen for stimulating discussion.

References

1. cf. Klaus Vetter, Elektrochemische Kinetik, Springer 1961, p. 513.
2. J.O.M. Bockris and A.K.M. Huq, Proc. Roy. Soc., A 237, 277 (1956).
3. N. Watanabe and M.A.V. Devanathan, J. Electrochem. Soc. 111, 615 (1964).
4. J.P. Hoare, J. Electrochem. Soc. 110, 1019 (1963).
5. J.O.M. Bockris and L.F. Oldfield, Trans. Faraday Soc. 58, 249 (1955).
6. Ref. 1, p. 500.
7. Y.L. Sandler and S.Z. Beer, "A Study of the Adsorption Mechanism on Oxygen Electrodes," Final Report, March 1964, Contract DA-36-039 AMC-00136(E).
8. H.G. Bain, Trans. Electrochem. Soc. 78, 173 (1940).
9. D. Winkelmann, Z. Elektrochemie 60, 738 (1956).
10. R. and H. Gerischer, Z. Phys. Chemie (N.F.) 6, 178 (1956).
11. W.G. Berl, Trans. Electrochem. Soc. 83, 253 (1943).
12. W.M. Latimer, Oxidation Potentials, Second Edition, Prentice-Hall, New York (1953).
13. M.W. Breiter, Electrochimica Acta, 9, 441 (1964).
14. Y.L. Sandler and D.D. Durigon, forthcoming publication.

Figure Captions

Fig. 1 Cathodic polarization curves of a chemically pretreated electrode; I - first polarization curve; II - after ...$^{-4}$ Amp/cm^2 overnight (■ overshoot on decreasing current); III - after anodization at 1.8 Volt.

Fig. 2 Polarization curves after thermal gas pretreatments of electrodes: 1 - after hydrogen pretreatment; 2 - after oxygen pretreatment. c = cathodic, a = anodic.

Fig. 3 Polarization curves with oxygen and with hydrogen pretreated foils in anodically pre-electrolyzed 1N perchloric acid. Anodic curves taken first. Cathodic curves shown for increasing and decreasing currents.

Fig. 4 Decay curves at varying peroxide concentrations.

Fig. 5 Cathodic polarization curves at various added concentrations of peroxide:

I. Hydrogen pretreated electrode:

(a) 10^{-3} M H_2O_2, He - saturated solution

(b) 10^{-3} M, O_2 in solution

(c) 10^{-4} M H_2O_2, He

(d) 10^{-4} M H_2O_2, O_2

II. Oxygen pretreated electrode:

(e) 10^{-4} M H_2O_2, He

Figure Captions (cont'd)

Fig. 6 Cathodic polarization curves at 10^{-5} M H_2O_2 (a) He (b) O_2 - atmosphere.

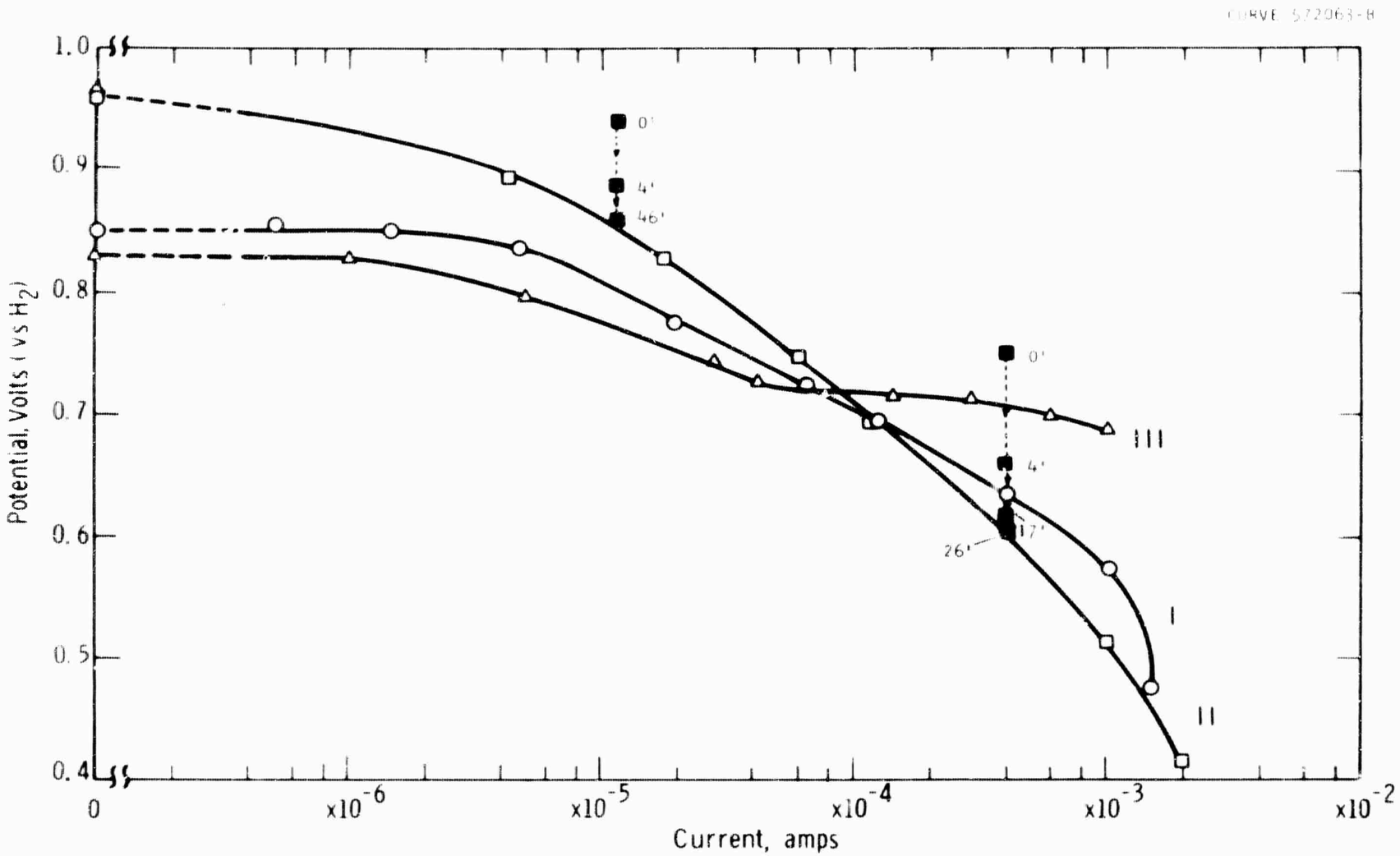
CURVE 572063-B
1.0
0.9
0.8
0.7
0.6
0.5
0.4
Potential, Volts (vs H_2)
0
$x10^{-6}$
$x10^{-5}$
$x10^{-4}$
$x10^{-3}$
$x10^{-2}$
Current, amps
0'
4'
46'
0'
4'
17'
26'
I
II
III

Fig. 1

Fig. 3

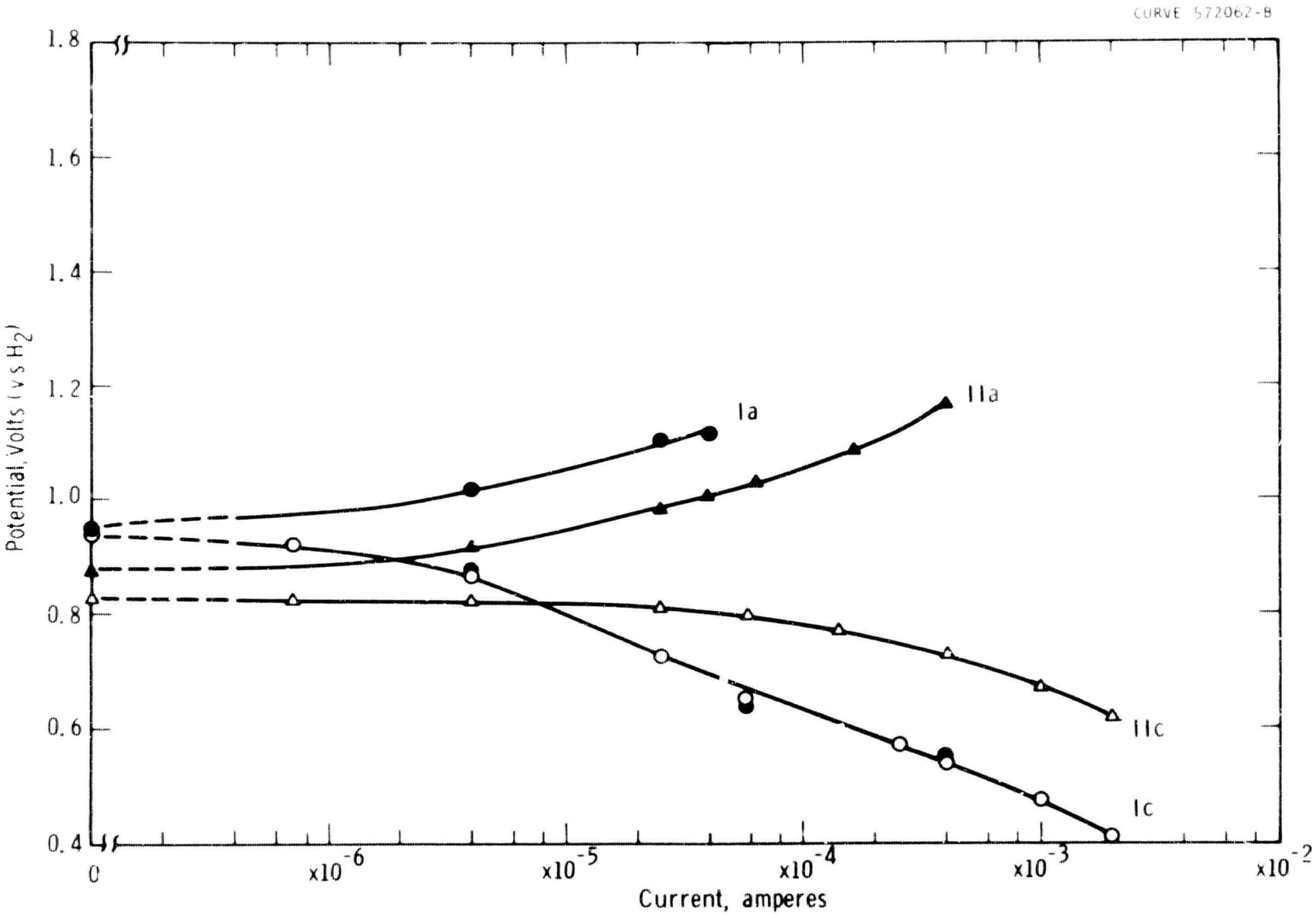
CURVE 572062-B
1.8
1.6
1.4
1.2
1.0
0.8
0.6
0.4
Potential, Volts (vs H_2)
Ia
IIa
IIc
Ic
0
x10^{-6}
x10^{-5}
x10^{-4}
x10^{-3}
x10^{-2}
Current, amperes

Fig. 2

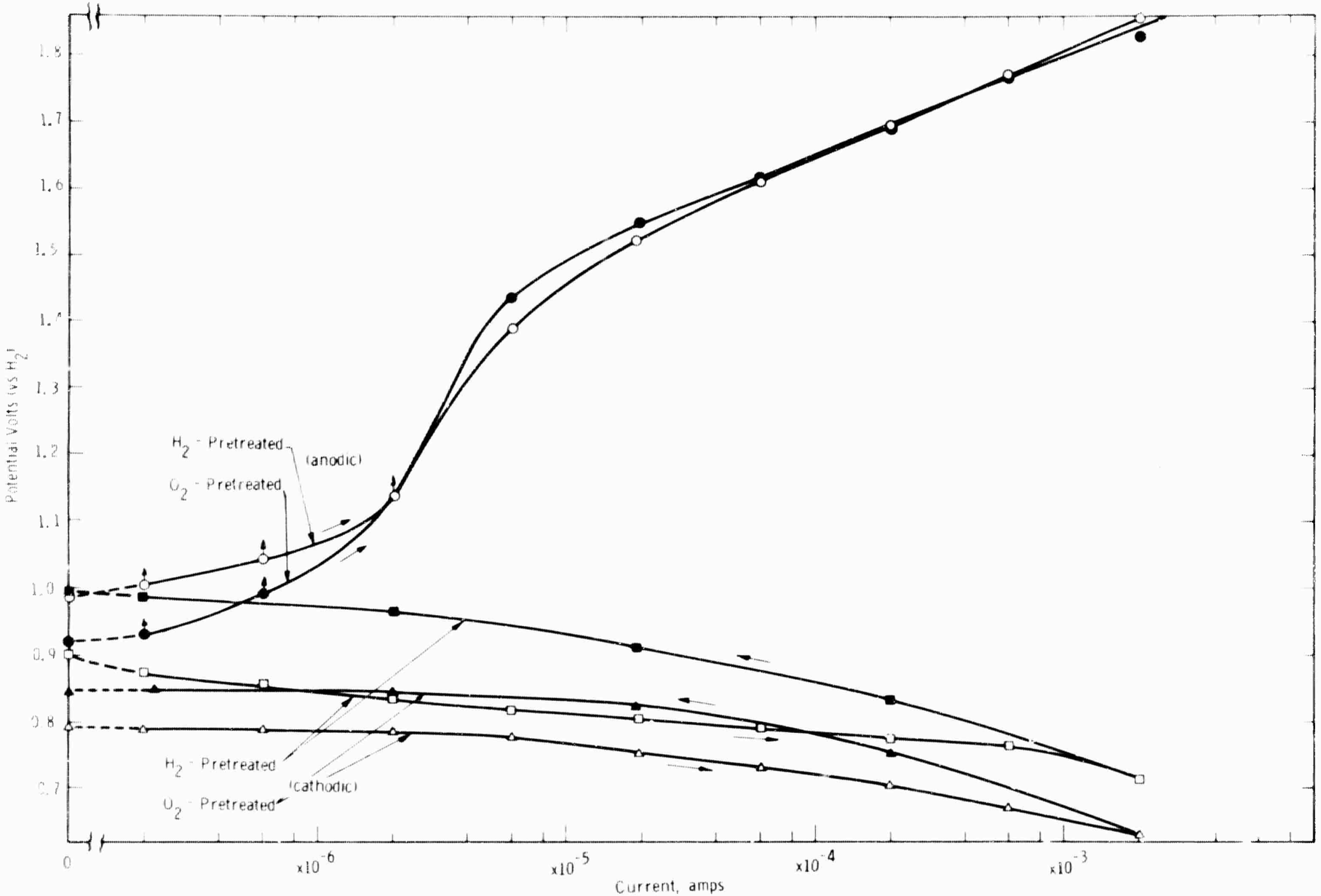
1.8
1.7
1.6
1.5
1.4
1.3
1.2
1.1
1.0
0.9
0.8
0.7
Potential Volts (vs H_2)
H_2 - Pretreated
(anodic)
O_2 - Pretreated
H_2 - Pretreated
(cathodic)
O_2 - Pretreated
0
$\times 10^{-6}$
$\times 10^{-5}$
$\times 10^{-4}$
$\times 10^{-3}$
Current, amps

Fig. 3

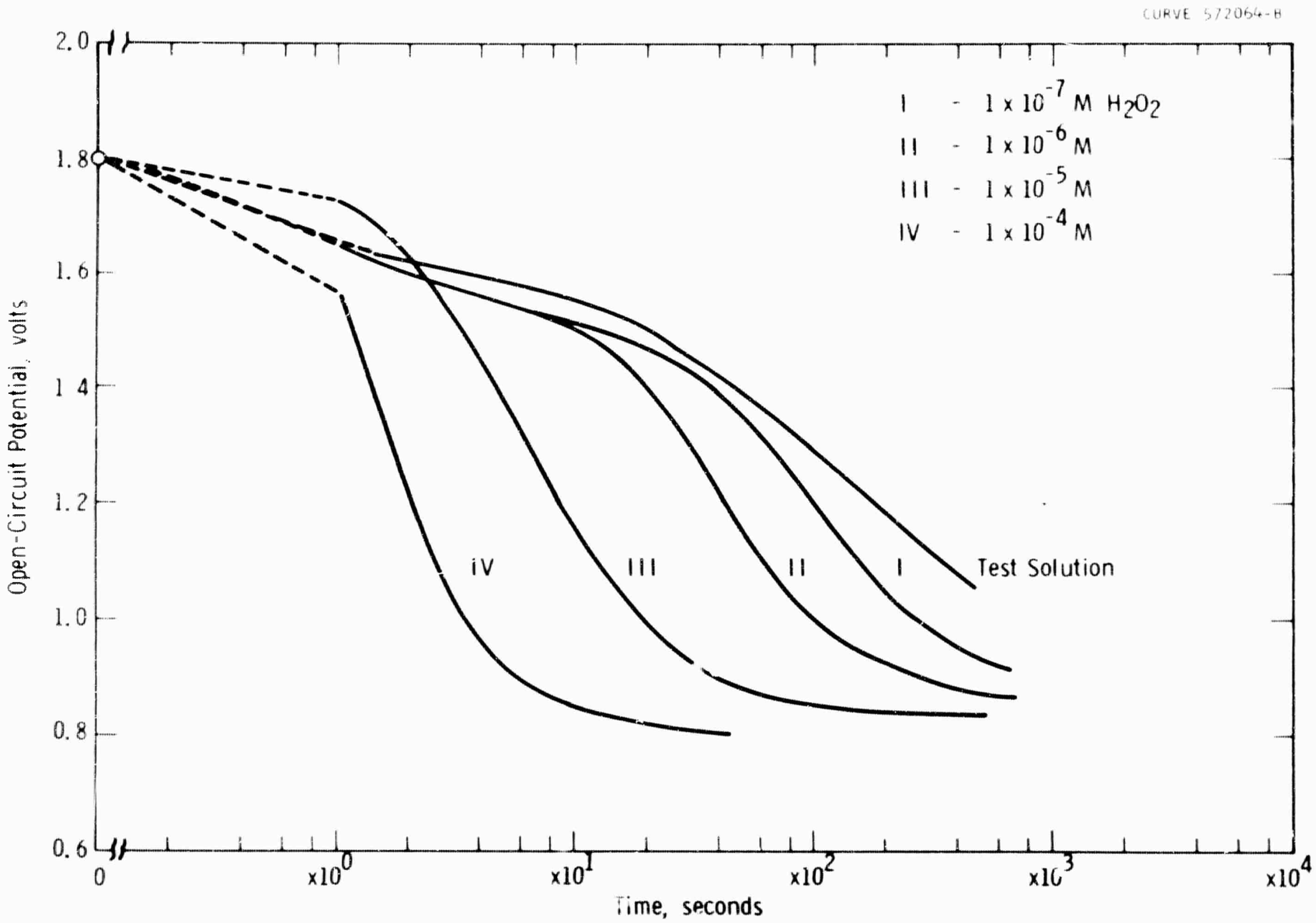
CURVE 572064-B
2.0
1.8
1.6
1.4
1.2
1.0
0.8
0.6
Open-Circuit Potential, volts
I - 1 x 10^-7 M H2O2
II - 1 x 10^-6 M
III - 1 x 10^-5 M
IV - 1 x 10^-4 M
IV
III
II
I
Test Solution
0
x10^0
x10^1
x10^2
x10^3
x10^4
Time, seconds

Fig. 4

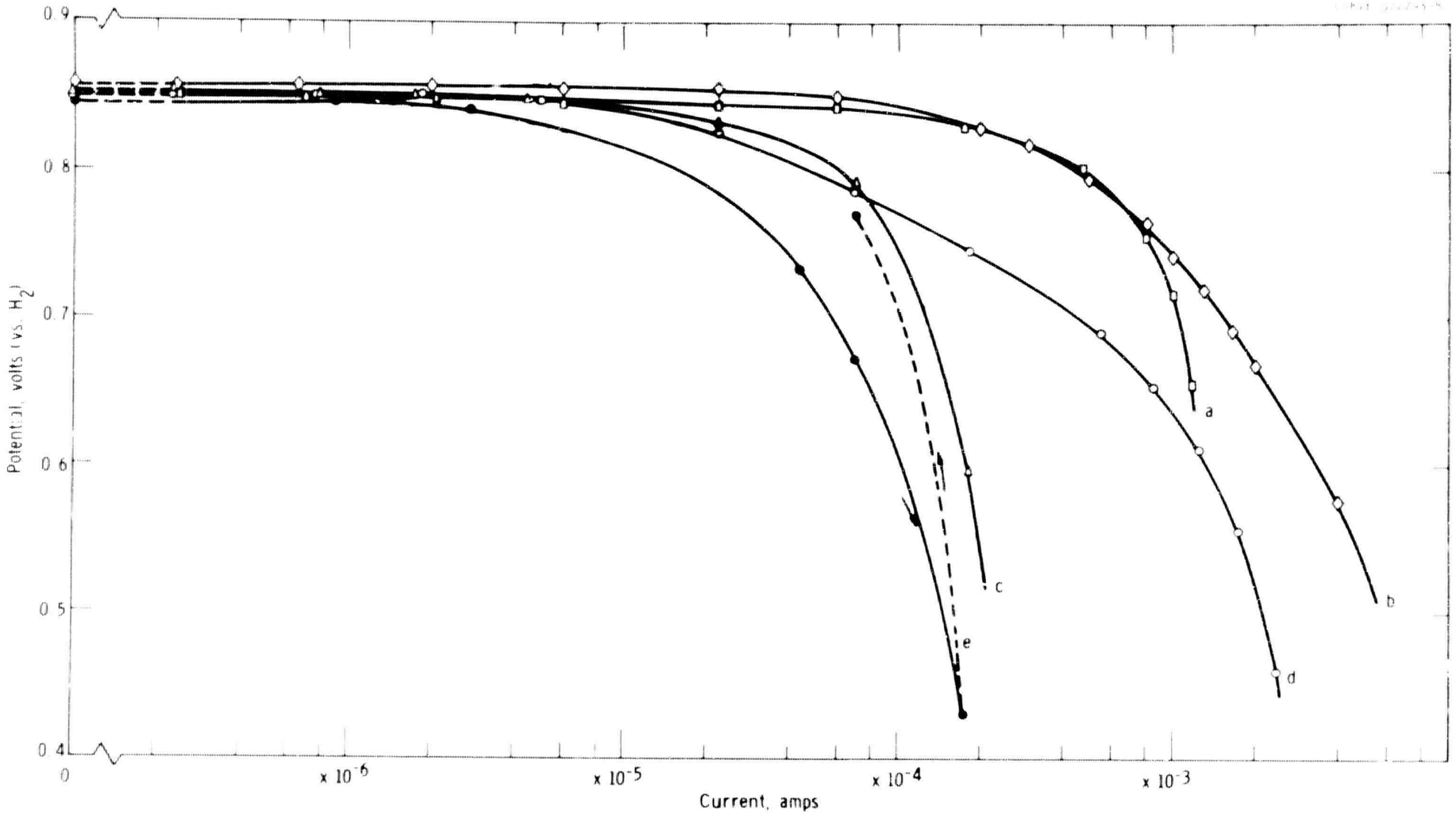
0.9
0.8
0.7
0.6
0.5
0.4
Potential, volts (vs. H_2)
0
x 10^{-6}
x 10^{-5}
x 10^{-4}
x 10^{-3}
Current, amps
a
b
c
d
e

Fig. 5

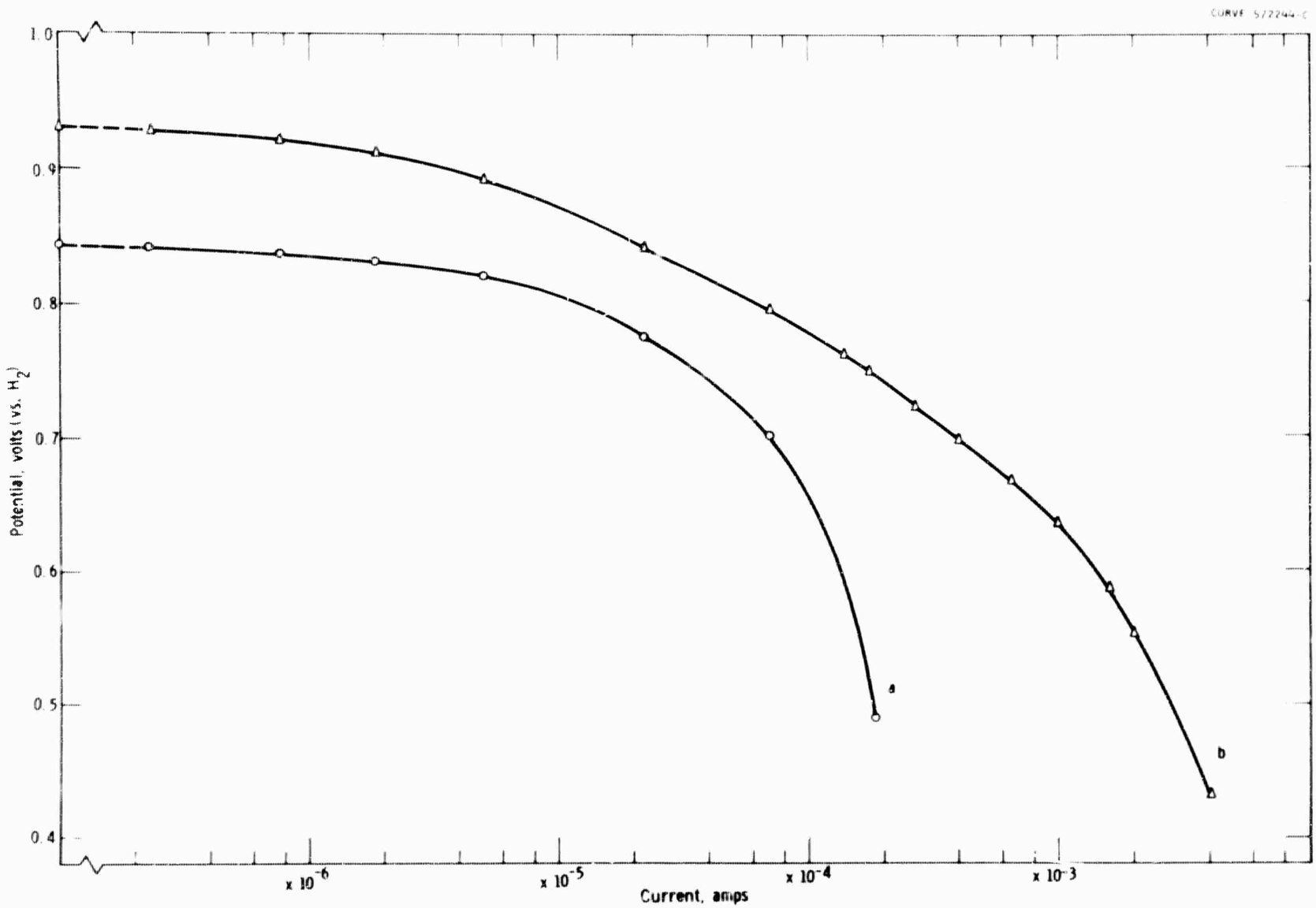
CURVE S72244-C
1.0
0.9
0.8
0.7
0.6
0.5
0.4
Potential, volts (vs. H_2)
x 10^{-6}
x 10^{-5}
x 10^{-4}
x 10^{-3}
Current, amps
a
b

Fig. 6

CONDUCTIVITY PROCESSES AT HIGH DOPING LEVELS

R. R. Heikes

In many transition metal compounds, particularly many of the oxides, it is felt that the charge carriers are best treated as occupying localized states associated with a lattice site rather than Block states in a conduction band. The conduction process is then treated as a thermally activated diffusion of the charge carriers from site to site. The measured activation energy for conduction is composed of two terms: (1) the energy required to free the charge carrier from its impurity and (2) the energy associated with the hopping process from site to site.

Unfortunately very low mobilities are normally associated with this type of conduction process. Therefore, standard semiconductor measurements such as Hall coefficient, magnetoresistance, or cyclotron resonance are presently either difficult or impossible to perform. In fact, from what follows, it will be seen that even when one can measure a Hall voltage, the interpretation is not straightforward. Partly as a consequence of this low mobility one tends to work at much higher doping levels than in diamond type semiconductors. Doping levels as high as 10% are not uncommon. It is the purpose of this paper to investigate the transport properties at such high doping levels.

The questions arising at high doping concentrations can best be introduced by examining some experimental data. First, consider the activation energy for conduction as a function of doping concentration.

Normally one finds that with increasing concentration the activation energy first drops off rapidly and then levels off for doping concentrations above several percent. Second, consider the Seebeck coefficient at high concentrations. The theory of the Seebeck coefficient for localized carriers indicates that, at high temperatures, it should be equal to the entropy of mixing for the charge carriers, that is a function of the ratio of the number of available sites to the number of charge carriers. However, the experimental values always turn out to be significantly lower. Qualitatively one can understand these data if one makes the reasonable hypothesis that the charge carriers prefer to occupy sites having the largest number of impurity nearest neighbors. Now at a concentration of say 5% approximately 50% of the lattice sites have impurity atoms as nearest neighbors. Thus, it is possible for a charge carrier to pass through the lattice without freeing itself from the impurity, that is, always remaining n-n to an impurity. Therefore, the measured activation energy should become simply that for the hopping process and thus qualitatively we may understand the behavior of the activation energy as a function of doping concentration. The Seebeck coefficient also follows simply. For now the number of available sites for the charge carriers has been reduced by a factor of the order of 2. This factor appropriately lowers the calculated Seebeck coefficient to be in accord with experiment.

Thus, we see that the idea of preferred regions or paths in the crystal appears to give a qualitative account of the situation; however, before we can accept this point of view, we must show that it can be

put into quantitative accord with experiment. Because of the number of simplifying assumptions that must go into the normal theoretical attacks of transport calculations, we decided to go instead to the Monte Carlo techniques using a high speed computer. In this way we have the opportunity of determining the results of our model, as accurately as we desire, or rather as accurately as our budget will allow.

The calculation is done in the following manner. We consider a crystal containing approximately 16000 lattice sites, and we use periodic boundary conditions. Actually the size of the lattice to be studied is determined by the size of the computer memory. Each lattice site is associated with a particular storage location in the computer memory. At any given time the storage location can tell us whether that lattice site is occupied by a host atom, impurity atom or a charge carrier. We must first place the desired number N of dopant atoms in the crystal. For concreteness we will treat only the donor case. This is done by asking the computer to choose N numbers at random between 1 and 16000. A dopant atom is associated with each site so chosen. The electrons, originating from the donors are then similarly placed. However, such a random placement of electrons is equivalent to having the system at infinite temperature, so that it is now necessary to bring the electron distribution to the desired temperature. To do this one only needs to give the electrons the rules for hopping and allow the hopping to continue until equilibrium is attained, that is, until the energy is constant within the calculable statistical fluctuation. In practice the hopping

procedure is as follows. The computer chooses (1) a charge carrier at random and (2) a neighboring atom at random. If the neighboring site so chosen is occupied by either a dopant atom or an electron, a jump is forbidden and the computer chooses another electron at random. If, on the other hand, this site is available to the electron, the computer then evaluates the electrostatic energy of the crystal with the electron or the initial and the final site. The probability for a jump is then

$$P = e^{-(E_f - E_i)/kT}$$

where E_f and E_i are the electrostatic energies of the crystal with the charge carrier at the initial and final positions respectively. If $E_f \leq E_i$, P is set equal to unity. If this is not the case, the computer chooses a random number between zero and unity. If the number chosen is equal to or less than P the electron hops to the new site. If the number chosen is greater than P, the electron remains. As a rule of thumb, equilibrium is usually obtained when each carrier has made of the order of 25-30 jumps.

To determine the electrical conductivity we need only apply an electric field to our system. This is done by appropriately altering the probabilities for jumping parallel and antiparallel to the electric field. The electrical conductivity is then proportional to the ratio of the net number of forward jumps to the total number of attempts to jump.

To calculate the Peltier coefficient we simply need to determine the average energy of the charges carrying the current measured with respect to the chemical potential of the system. The chemical potential is easily determined by first calculating the energy of the original system as a function of temperature and then removing a small fraction of the electrons and redoing the calculation. The determination of the average energy of the charges carrying the current is easily carried out by keeping track of the energies of all the electrons as they jump.

Our program is to calculate the electrical conductivity, Seebeck coefficient and ultimately the Hall coefficient as a function of temperature for several concentrations. From this point on, the only real problem is the cost of computer time. The time consuming part of the computer program is the calculation of the energy of the system. As the interactions involved are electrostatic, the forces die off slowly. However, since the impurities are randomly located, the energy of the system will certainly converge if the range of the interaction used is of the order of the average spacing between impurities. An estimate of the computer time involved shows that the calculation is feasible. However, before going to this limit, we elected to do two simple and rather inexpensive cases to see if we could indeed expect our model to ultimately correspond to the real physical situation. The two cases we chose to treat were first considering only nearest neighbor interactions and second extending the range to include third nearest neighbors.

Now we ask, what are the general features that we want to see come out of such a calculation.

These general features are: (1) at concentrations above say 3-5%, we expect an activation energy, excluding the hopping contribution, small compared with the binding energy of an electron to an isolated impurity, (2) the Seebeck coefficient at high temperatures should be equal to the entropy of mixing for the electrons, where all are free, (3) as the temperature is lowered the Seebeck coefficient should first decrease slowly and finally increase rapidly with further lowering.

It is not surprising that both nearest neighbor and third nearest neighbor calculations give the correct Seebeck coefficient at high temperatures for here the electron distribution is random in either case and the energy of the system tends towards zero.

However, with regard to the activation energy, for nearest neighbor interactions only one finds a value nearly twice the binding energy of a carrier to an isolated impurity, whereas you will remember that we wish this value to be negligible. On the other hand, in the case of third nearest neighbors, the activation energy has been reduced to half the binding energy to an isolated impurity. If one considers a simplified model, these results are seen to be reasonable. Let us ask, at a concentrations of 10%, the one studied, how many sites in the crystal have zero, one, two, three, or four nearest neighbors of impurity. Since the impurities are located randomly, this is easily calculated. One finds that approximately 10% of the sites have three or more impurity neighbors. Thus, at lowest temperatures all the electrons can be accommodated in these sites. Now as the number of these sites is insufficient to form

continuous paths through the crystal, conduction can only take place by means of excitation to higher energy sites. Rough estimates indicate that only by including sites having only one impurity neighbor can one get continuous paths. Thus, we see that the minimum excitation for conduction to take place is from a site possessing three nearest neighbors to a site possessing one. The activation energy found on the computer for nearest neighbor interactions corresponds to this value. The considerable improvement in calculated activation energy on including third neighbors is clear when one considers that the energy level spacing is considerably reduced.

As similarly encouraging results were found for the Seebeck coefficient as a function of temperature, the calculation will be pursued to further neighbors.

A final remark, this type of calculation might be of interest to those interested in impurity band conduction in the hopping region.

BLANK PAGE

Scientific Paper 64-929-268-P1
Proprietary Class 3

April 3, 1964

DEFECT STRUCTURE AND ELECTRICAL CONDUCTIVITY OF ThO_2-Y_2O_3 SOLID SOLUTIONS*

E. C. Subbarao,** P. H. Sutter and J. Hrizo

Abstract

Compositions in the ThO_2-$YO_{1.5}$ system were co-precipitated as the oxalates and converted to the oxides. Disks were pressed and sintered in oxygen at 1400 to 2200°C Densities of the sintered disks were 96-98% of the theoretical. Solid solutions with the fluorite-type structure are formed up to 20-25 mole % $YO_{1.5}$ at 1400°C and up to 45-50 mole % $YO_{1.5}$ at 2200°C. Density data showed that these solid solutions correspond to $Th_{1-x}Y_xO_{2-0.5x}$, having a complete cation sublattice filled by Th^{4+} and Y^{3+} ions, and vacancies in the anion sublattice. The observed increase in electrical conductivity with increase in $YO_{1.5}$ content is consistent with charge transport by oxygen ions through a vacancy mechanism. Approximately 7 mole % ThO_2 is soluble in $YO_{1.5}$ at 2200°C. Density results indicate an anion interstitial structure for the Y_2O_3 phase Transference number measurements indicate that the electrical conductivities are only partially due to ions.

*Supported by ARPA through the U. S. Office of Naval Research.

**Now at Indian Institute of Technology, Kanpur, India.

I. INTRODUCTION

Thorium dioxide, ThO_2, has the cubic, CaF_2-type structure up to its melting point, ~3300°C. Yttrium sesquioxide, Y_2O_3 (or $YO_{1.5}$), crystallizes with the C-type rare earth oxide structure (or Tl_2O_3 type). This structure is closely related to that of CaF_2, from which it may be derived by an ordered omission of one-quarter of the anions and than a slight rearrangement of the atoms. Based on the similarity of the structure, extensive solid solution may be expected in the binary system ThO_2-$YO_{1.5}$. Hund and Mezger[1] found that 22 to 30 mole % $YO_{1.5}$ is soluble in ThO_2 at 1200°C.

The purpose of the present investigation is to determine the phase relations and solid solubility in the binary system ThO_2-$YO_{1.5}$ at temperatures up to 2200°C, to examine the defect structure of the resulting solid solutions and to present a preliminary account of the electrical conductivity measured on dense ceramic disks. Further details of the ionic conductivity of ThO_2 solid solutions will be discussed elsewhere.

II. SPECIMEN PREPARATION

Thorium nitrate and yttrium nitrate, obtained from Lindsay Division of the American Potash and Chemical Corporation, are the

starting materials. Spectrographic analyses of these materials are given in Table I. The nitrates were dissolved in distilled water and the oxide contents were determined by ignition at 1300-1400°C. The nitrate solutions were mixed in the required proportions to prepare the desired solid solution compositions. Thorium and yttrium salts can be precipitated either as (A) the hydroxide or (B) the oxalate.

(A) Hydroxide: In this method, described in detail by Hund and Mezger,[1] the heated nitrate solution was added to boiling ammonium hydroxide solution with vigorous stirring. The precipitate was filtered, washed and dehydrated at 105°C. After grinding, it was decomposed to the oxides at 1200°C. The oxide mixture was ground, pressed into disks and the disks were sintered at temperatures between 1400° and 2000°C. The densities of disks that were prepared from the hydroxide and from the oxalate are compared in Table II. The densities were determined from the mass and the dimensions. Inasmuch as the oxalate method led to higher densities, the hydroxide method was discarded.

(B) Oxalate: Since the particle size distribution of the starting oxide powder has a remarkable influence on the sintering behavior of the oxide, it is advantageous to obtain fine-grained oxides. In a sintering study of thoria obtained from the hydroxide, carbonate, nitrate, and oxalate, Kantan et al[2] concluded that the oxalate method yielded the maximum density.

In this method, the nitrate solutions were placed in an ice bath. Saturated oxalic acid was added drop by drop while the chilled nitrate solution was vigorously stirred. Beyond this step, two courses were available: (1) dehydration of the entire solution, or (2) filtration and dehydration of the precipitate.

(1) The entire solution was dehydrated at about 120°C, leaving a cake at the bottom of the beaker. The top surface of the cake was more granular than the bottom. This difference in grain size became more pronounced on heating at about 900°C. X-ray diffraction studies of the different portions of the cake indicated the granular material at the top of the cake to be mostly $YO_{1.5}$ and the fine material at the bottom to be essentially ThO_2. The reasons for segregation and grain growth of $YO_{1.5}$ are not clear at present. Disks, pressed from this powder without much grinding, had an inhomogeneous appearance after firing to 2000°C for 4 hrs. White specks (of Y_2O_3) were randomly distributed throughout the volume of the disk. Careful grinding was necessary to obtain homogeneous solid solutions from material prepared by this method.

(2) The precipitate was filtered, taking care to avoid segregation in the beaker, washed until the precipitate was free of acids, and then dehydrated at about 120°C. The resulting fine-grained oxalates were calcined to the oxides at 900°C[3,4] for 8-12 hrs. The

oxide powder was homogeneous and fine-grained. This method gave satisfactory results and was therefore followed in the rest of the investigation.

The powder was ground and pressed into disks, 3-12.5 mm in diam. and 1-10 mm in thickness at a pressure of about 20,000 psi. After precalcination at 1400°C for 4 hrs., the specimens were sintered in an oxygen atmosphere in the temperature range 1600 to 2200°C for 3 to 7 hrs. During sintering, the specimens were enclosed in covered thoria crucibles to avoid contact with undesirable vapor species that may be present in the furnace chamber. To prevent the disks from sticking to each other during sintering, they were separated using powders sintered at 2250°C as spacer material.

The ThO_2 solid solution compositions sintered in oxygen range in color from ivory white to brown, the intensity of the brown color increasing with $YO_{1.5}$ for a given sintering temperature.

Typical microstructures of polished and etched surfaces of the sintered specimens are shown in Fig. 1. The pure thoria was etched by hot phosphoric acid and the others by hot sulfuric acid. The grain size of all of the specimens is of the order of 20 microns, and increases slightly with increasing $YO_{1.5}$ content. The pore size also appears to increase with $YO_{1.5}$ content. The porosity has been roughly estimated at 2-4 percent in the specimens with 0 to 15 mole percent $YO_{1.5}$, the higher porosity applying to the higher $YO_{1.5}$ content.

III. PHASE RELATIONS

Specimens that had been sintered between 1400°C and 2200°C for 3 to 6 hours in an oxygen atmosphere were cooled in the furnace. X-ray examination of the sintered specimens, using CuKα radiation, was used to determine the phases present.

The system may conveniently be divided into three regions: ThO_2-type solid solutions, Y_2O_3-type solid solutions and a two phase region separating these two solid solutions. Solid solutions with the fluorite-type structure were found up to 50-55 mole % $YO_{1.5}$ at 2200°C. The phase boundary decreased to 20-25 mole % $YO_{1.5}$ at 1400°C, which is consistent with Hund and Mezger's results.(1) Y_2O_3-type solid solutions were present up to 7 mole % ThO_2 in $YO_{1.5}$ at 2200°C, decreasing to about 3 mole % ThO_2 at 1400°C. The solubility limit was determined from the variation with composition of the interplanar spacing from several back reflection lines, as shown in Fig. 2 for specimens sintered at 2200°C. The solubility limits are believed to be accurate within ± 3 mole %. The sub-solidus phase relationships in the system are summarized in Fig. 3.

The lattice parameters of specimens sintered at 2200°C are plotted in Fig. 4. The values were obtained from diffraction lines with $2\theta > 100^\circ$ and were extrapolated according to the method of Nelson and Riley.(5) The variation of lattice constant with composition can be accounted for by the relative size of the ions (Y^{3+} = 0.92 A, Th^{4+} = 0.99 A).

The lattice parameters of ThO_2 and Y_2O_3 that were obtained here are in good agreement with published values.[6] Those of the ThO_2-type solid solutions are slightly smaller than Hund and Merger's values.

IV. DEFECT STRUCTURE AND ELECTRICAL CONDUCTIVITY

When the Th^{4+} ions are replaced by Y^{3+} ions, charge neutrality can be restored by one of two structural schemes: (1) The cation sublattice is completely filled by Th^{4+} and Y^{3+} ions and the appropriate number of anion vacancies are created. (2) The anion sublattice is complete and the excess cations occupy interstitial sites. In order to distinguish between these two models, densities corresponding to them are computed using the lattice parameters shown in Fig. 4. These density values are compared in Fig. 5 with those measured pycnometrically on powders which had been sintered at 2200°C. On the basis of these data, it was concluded that the ThO_2 solid solutions have fluorite type structure with a filled cation sublattice and anion vacancies.

The densities of sintered disks which were used for conductivity measurements, were measured by a displacement method using dibutyl phthalate. These values are also included in Fig. 5 and show that these specimens have a porosity of 1-5%, in agreement with the photomicrographic study.

It has been pointed out that the structure of Y_2O_3 may be derived from the fluorite structure by an ordered omission of one-quarter

of the oxygen ions. The introduction of ThO_2 into the Y_2O_3 lattice may result in one of the following structural schemes, assuming the substitution of the Th^{4+} in Y^{3+} sites and no valence change: (1) Anion interstitial model: Completely filled cation sublattice with excess anions, which are required for charge neutrality, filling some of the ordered anion vacant sites in the Y_2O_3 structure. (2) Cation vacancy model: Anion sublattice the same as in Y_2O_3 and with cation vacancies created to preserve electrical neutrality. It is possible to choose between these two models by comparing the density calculated from the measured x-ray lattice parameter with the macroscopic density. Sintered samples of pure Y_2O_3 and the solid solution of 5 mole % ThO_2 in $YO_{1.5}$ were crushed to powder and powder densities were determined by displacement with dibutyl phthalate. A number of measurements were made in which the determinations were made in pairs in such a way that the ratio of the densities of the pure Y_2O_3 and the solid solution is more accurate than the separate values. The measured x-ray lattice parameter yields a computed ratio of 1.039 for the cation vacancy model and 1.056 for the anion interstitial model. The ratio of the macroscopic densities was $1.07 \pm .005$. This value is higher than either of the models predicts. This may be due to a residual porosity in the fairly coarse powder used, with a greater porosity in the pure Y_2O_3 than in the solid solution because of improved sintering in the latter. This effect may account

for the deviation above the anion interstitial model but we do not believe that it would cause the deviation from the value corresponding to the cation vacancy model. Therefore, we conclude that the solid solution structure corresponds to the anion interstitial model.

The electrical conductivity of the sintered disks was measured in air at a frequency of 1000 cps with the use of a modified General Radio capacitance bridge in conjunction with decade resistance and capacitance boxes. Platinum paste electrodes were painted on the disks. The results for ThO_2 and for ThO_2 with 1, 2 and 5 mole % $YO_{1.5}$ are shown in Fig. 6 where log σT is plotted versus reciprocal absolute temperature in the range of 500 to 1400°C. The electrical conductivity increases with increasing $YO_{1.5}$ content. This behavior is consistent with the notion that the current carriers in these solid solutions are the oxygen ion vacancies and that the conductivity increases with anion vacancy concentration.

The measured electrical conductivity could contain contributions from ions, electrons or holes. Therefore, an experiment was performed to determine the fraction of the current that is due to ions. The transference number measurements were made by measuring the open circuit voltage across an oxygen concentration cell made up of a specimen disk with porous platinum electrodes painted on the center of each face. The disk was held between the ends of two alumina tubes which served to

contain the atmospheres of flowing oxygen on one face and flowing air on the other. A platinum-platinum rhodium thermocouple contacted each electrode and the platinum legs were brought out to a precision potentiometer that was used to measure the emf across the cell. A furnace heated the apparatus up to a maximum temperature of 1400°C. At each temperature the oxygen and air atmospheres were reversed in order to eliminate small Seebeck voltage and other stray voltages. For a completely ionic conductor the theoretical emf across an oxygen gas concentration cell is $(RT/4F)\ln P_2/P_1$ where R is the gas constant, F is the Faraday and P_2 and P_1 are the oxygen partial pressures or the two sides of the cell. If the contribution of electrons and holes to the conductivity is appreciable, the measured open circuit voltage is less than the theoretical value. The ionic transference number is equal to the ratio of the measured voltage to the theoretical voltage. The apparatus was checked by measuring the transference number of 13 mole % $CaO-ZrO_2$. From 800 to 1400°C the ionic transference number was found to be $1.00 \pm .005$ indicating essentially 100% ionic conductivity as expected. For the $ThO_2-YO_{1.5}$ system samples, the ionic transference number results indicated a large contribution of electrons or holes to the conductivity. There was considerable scatter in these results but typical values are shown in Table 3. It is now known whether this electronic conductivity is due to impurities, despite our very pure starting materials, or some other cause. A test of the effect of measuring the conductivity

in air and oxygen showed that the conductivity increased with increasing oxygen partial pressures, implying hole conduction.

The electrical conductivity of the Y_2O_3 is included in Fig. 6 and indicates an activation energy of 1.9 ev, which is higher than the value of 1.46 ev that was reported by Nodack and Walch[7] in the same temperature region. The reason for this discrepancy is not known. The density measurements that were described above showed that the solid solution of thoria in yttria had the anion interstitial structure. With this structure, the ionic conductivity is accounted for by the oxygen ions. It should be mentioned, however, that Berard and Wilder[8] have measured the diffusion coefficient of yttrium in quite porous Y_2O_3 to be 3×10^{-10} $cm^2/sec.$ at 1400°C. Use of the Einstein relation yields a calculated electrical conductivity that is about 1% of the measured electrical conductivity in the Y_2O_3. If the addition of ThO_2 to Y_2O_3 were to yield cation vacancies, contrary to the above conclusion of an anion interstitial structure, then the cation conductivity might well be increased enough to also account for the higher ionic transference number in the 95% $YO_{1.5}$ solid solution as shown in Table III. In order to establish the defect structure and conductivity mechanism in rare-earth sesquioxides, some other system such as La_2O_3-ZrO_2 in which the solubility limit is more extensive would be useful. A comparison of the cation diffusion rate in the pure material and the solid solutions would be informative.

REFERENCES

1. F. Hund and R. Mezger, "The Fluorite Phase in the System ThO_2-Y_2O_3. Its Defect Ordering, Electrolytic Conductivity and Irregular Lattice Disorder," Z. Physik. Chem. 201, 268 (1952).

2. S. K. Kantan, R. V. Raghavan, and G. S. Tendolkar, "Sintering of Thorium and Thoria," Proc. U. N. Intern. Conf. Peaceful Uses Atomic Energy, 2nd, Geneva, 1958, 6, 132.

3. R. W. M. D'Eye and P. G. Sellman, "The Thermal Decomposition of Thorium Oxalate," J. Inorg. Nucl. Chem. 1, 143 (1955).

4. Y. Harada, Y. Baskin, and J. H. Handwerk, "Calcination and Sintering Study of Thoria,", J. Am. Ceram. Soc. 45, 253 (1962).

5. J. B. Nelson and D. P. Riley, "An Experimental Investigation of Extrapolation Methods in the Derivation of Accurate Unit-Cell Dimensions of Crystals," Proc. Phys. Soc. (London) 57, 160 (1945).

6. (a) H. E. Swanson and Eleanor Tatage, "Standard X-ray Diffraction Powder Patterns," N.B.S. Circular 539, Vol. I (1953) p. 57.
(b) H. E. Swanson, Ruth K. Fuyat, and G. M. Ugrinic, "Standard X-ray Diffraction Powder Patterns," N.B.S. Circular 539, Vol. III (1954) p. 28.

7. W. Noddack and H. Walch, "On the Electrical Conductivity of Oxides," Z. Elektrochem. 63, 269 (1959).

8. M. F. Berard and D. R. Wilder, "Self-Diffusion in Polycrystalline Yttrium Oxide," J. Appl. Phys. 34, 2310 (1963).

Table I -- Spectrographic Analyses of Starting Materials

$Th(No_3)_4$		$Y(No_3)_3$	
Element	ppm	Element	ppm
Bi	< 1	Mg	20
Ca	2.5	Si	200
Cu	2	Fe	200
In	< 1	Mn	50
Mg	3	Ca	< 100
Nb	< 2	Al	50
Pb	< 1	Cu	< 100
Si	15	Ti	50
Sn	< 1	Co	< 100
Ti	< 2	Ni	< 100
U	< 100		
W	< 30		
Zn	< 10		
Zn	3		
Y	< 2		
Ce	< 200		
Au	< 10		
Ba	< 3		
K	< 6		
Na	3		
P	< 50		
Sb	< 1		
Sn	< 1		

Table II -- Densities of Sintered Thoria Specimens

Sintering Conditions	Hydroxide (Calcined at 600°C - 8 hrs.)	Oxalate (Calcined at 900°C - 12 hrs.)
1200°C - 2 hrs.	7.4 g cm^{-3}	7.3 g cm^{-3}
1400°C - 2 hrs.	7.5	7.8
1600°C - 2 hrs.	7.3	8.9
1800°C - 2 hrs.	7.9	9.7

Table III -- Ionic Transference Number

% $YO_{1.5}$	Temperature, °Centigrade 1000	1200	1400
0	.05	.09	.12
1	.25	.40	.45
2	.44	.50	.54
5	.63	.69	.69
95	.18	.27	.34
100	0	0	0

CURVE 567687-A

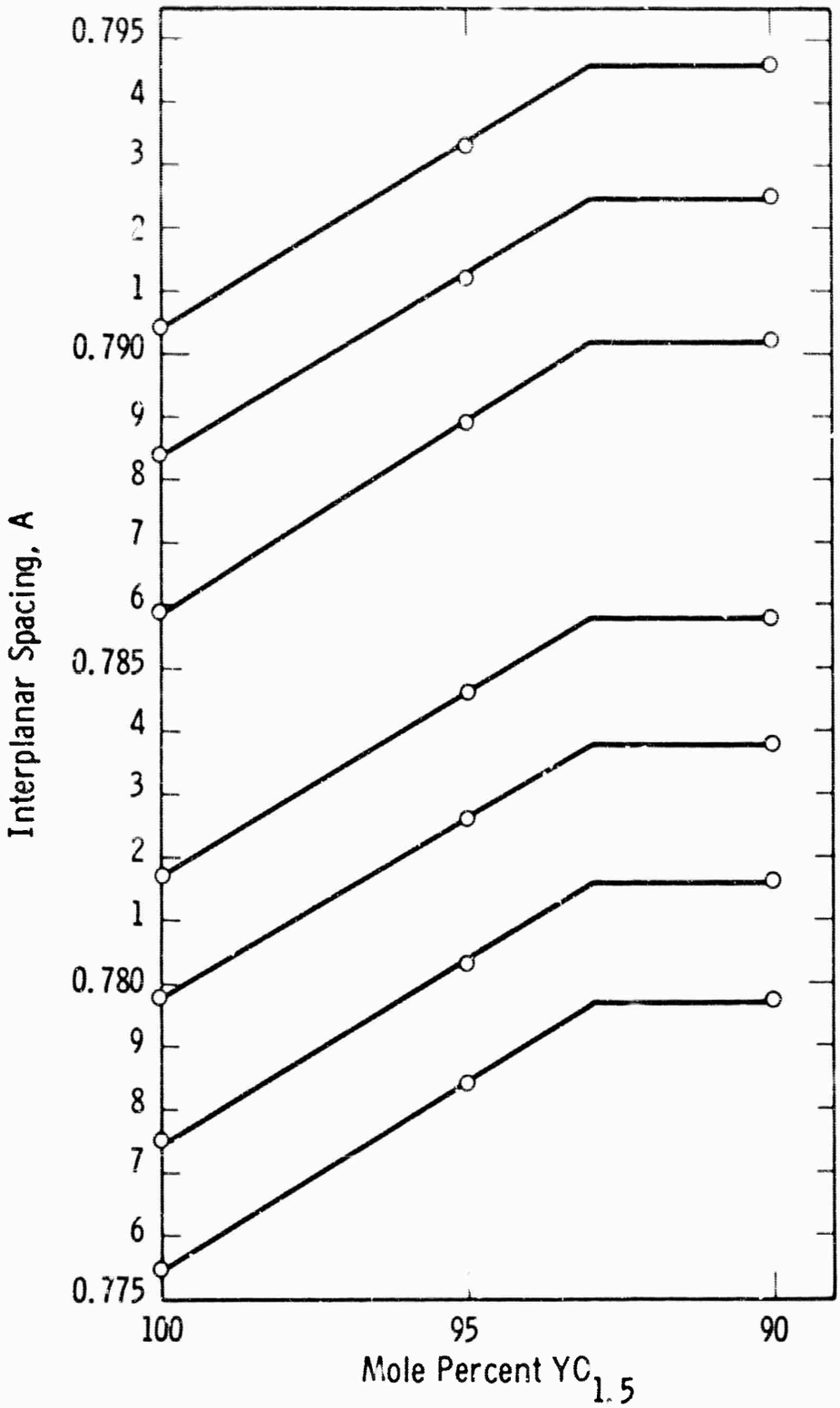

Fig. 2—Variation of interplanar spacing in the system ThO_2 - $YO_{1.5}$ (specimens sintered at 2200°C)

CURVE 567688-A

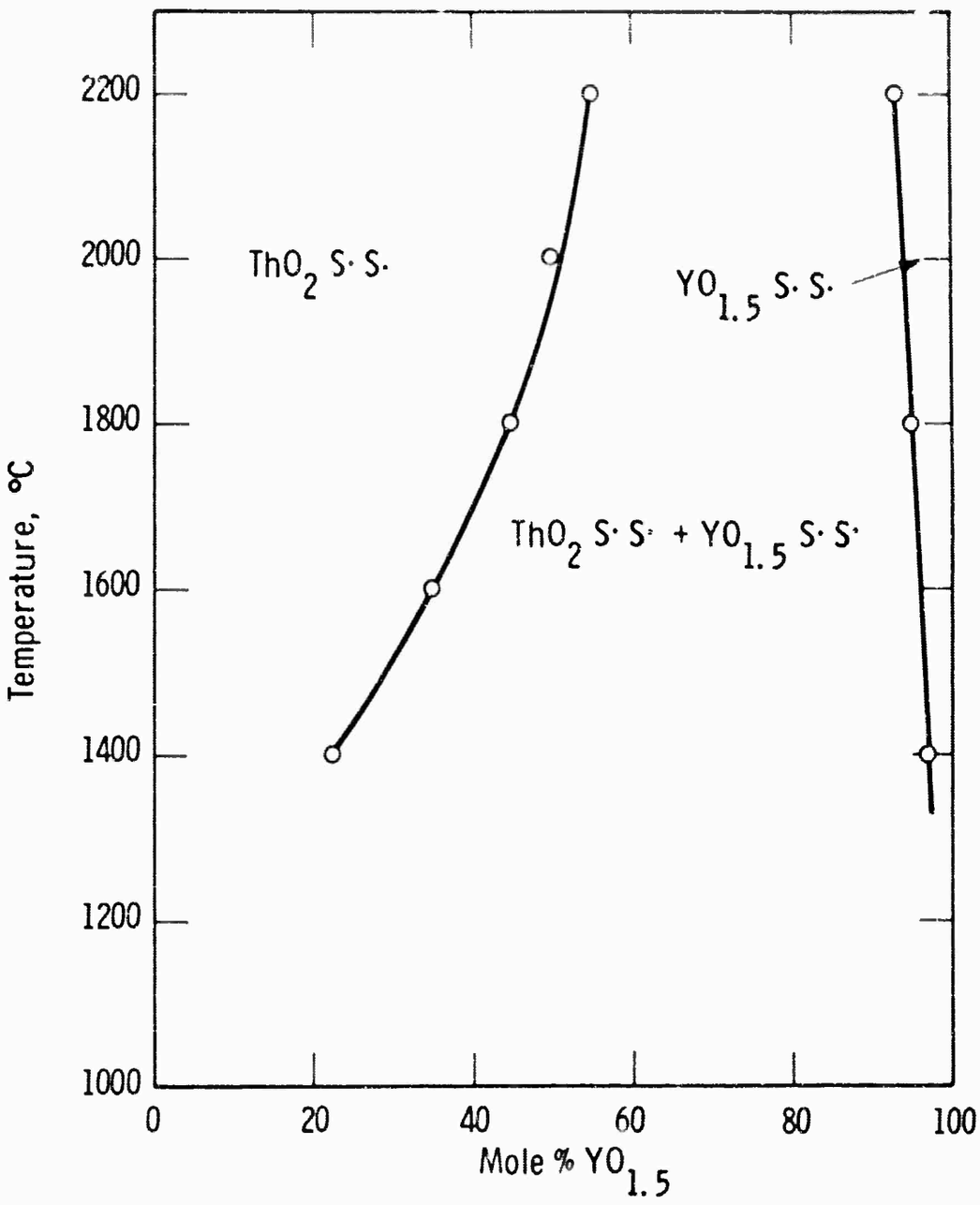

Fig. 3 — Sub-solidus phase relations in the system ThO_2 - $YO_{1.5}$

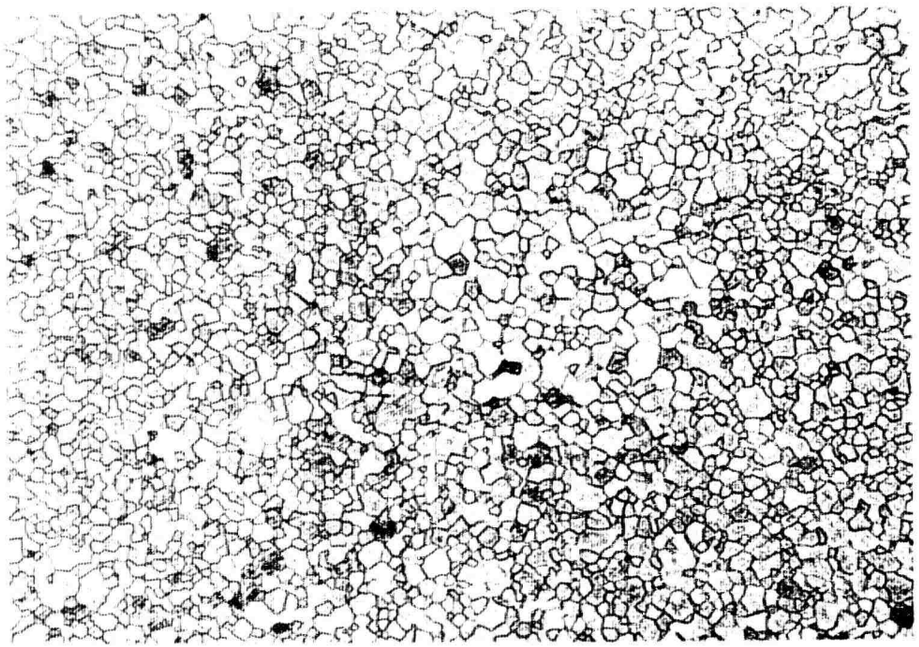

A

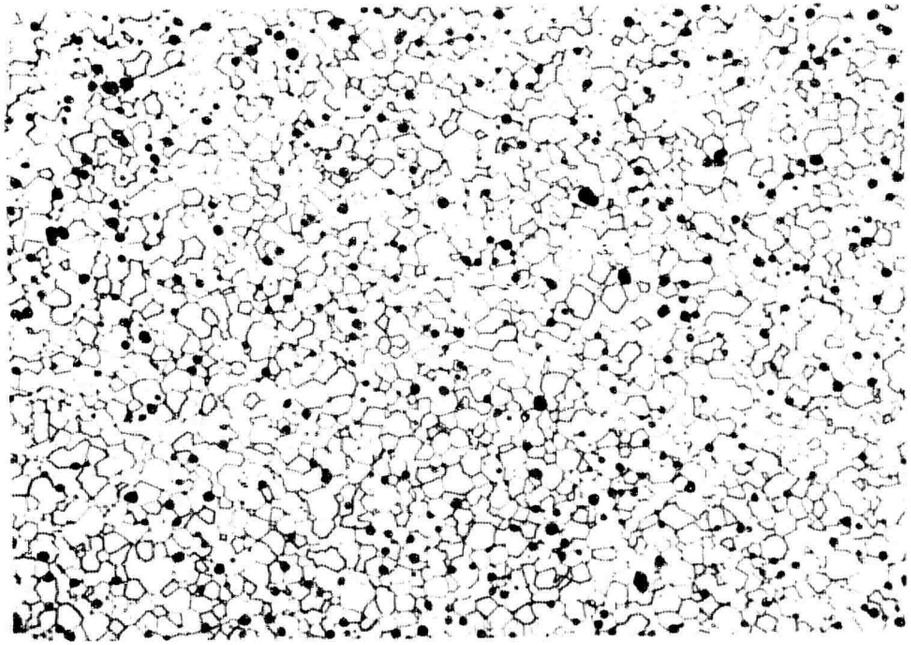

B

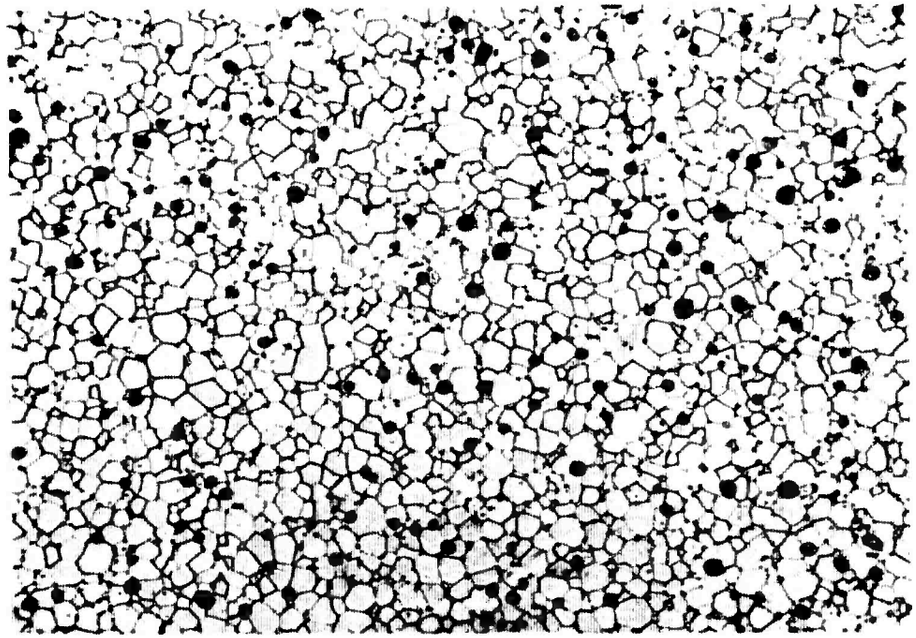

C

Fig. 1—Typical microstructures of ThO_2 - $YO_{1.5}$ solid solutions ceramics (2200 °C - 3 hrs)

A ThO_2

B 5% $YO_{1.5}$

C 15% $YO_{1.5}$

200 µ

BLANK PAGE

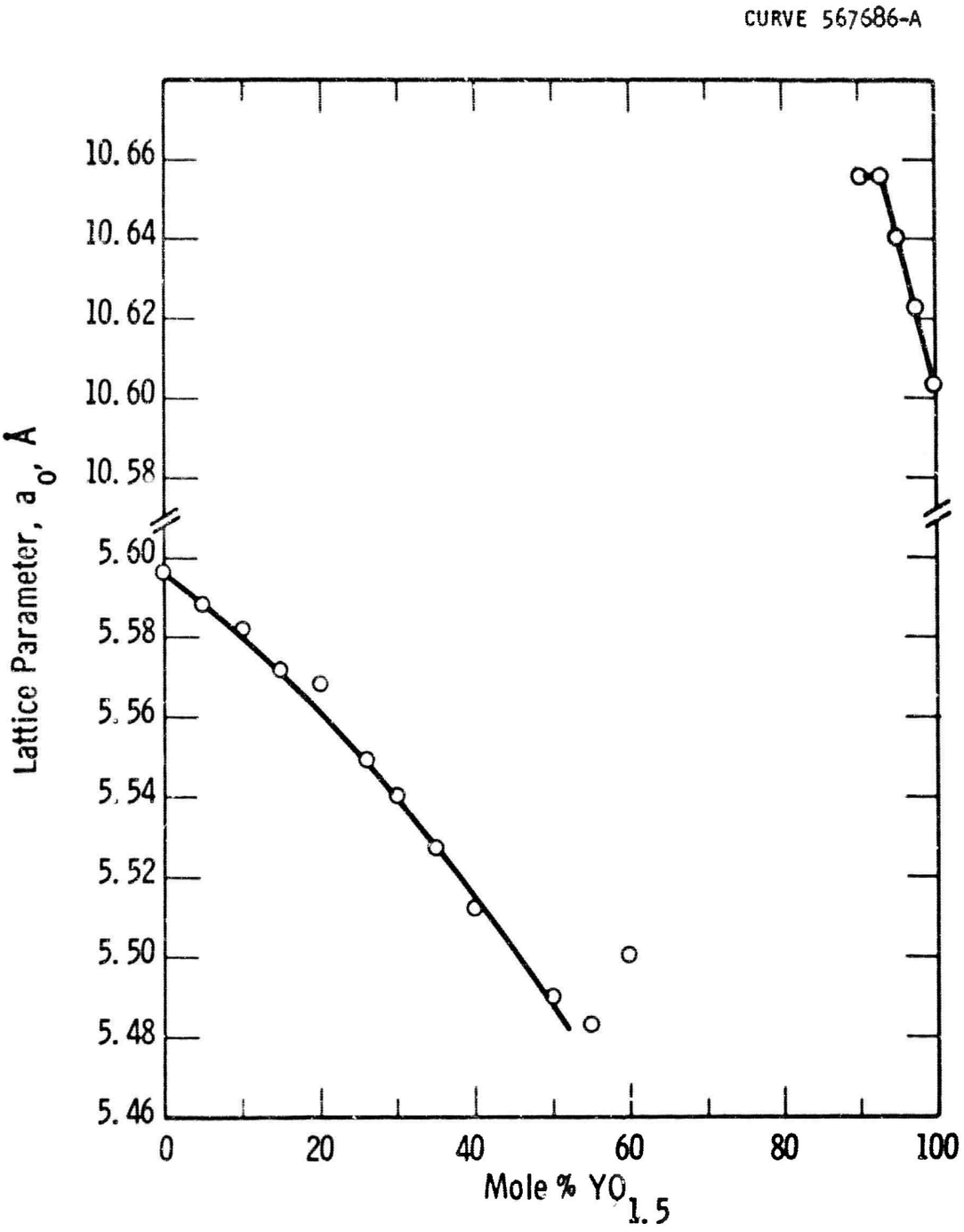

Fig. 4—Lattice parameters in the system ThO_2 - $YO_{1.5}$ (specimens sintered at 2200°C)

BLANK PAGE

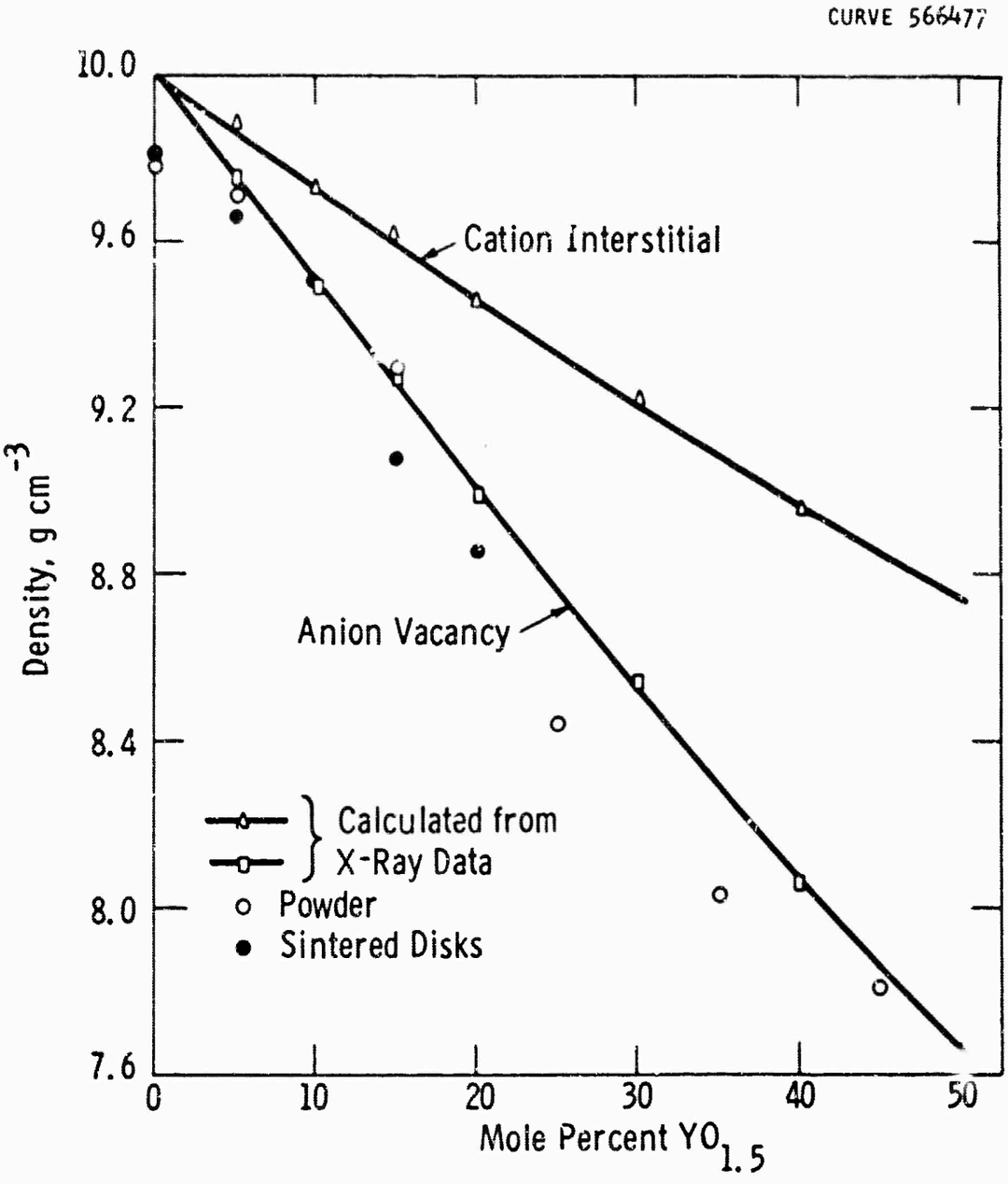

Fig. 5—Densities of ThO_2 - $YO_{1.5}$ solid solutions

CURVE 567689-A

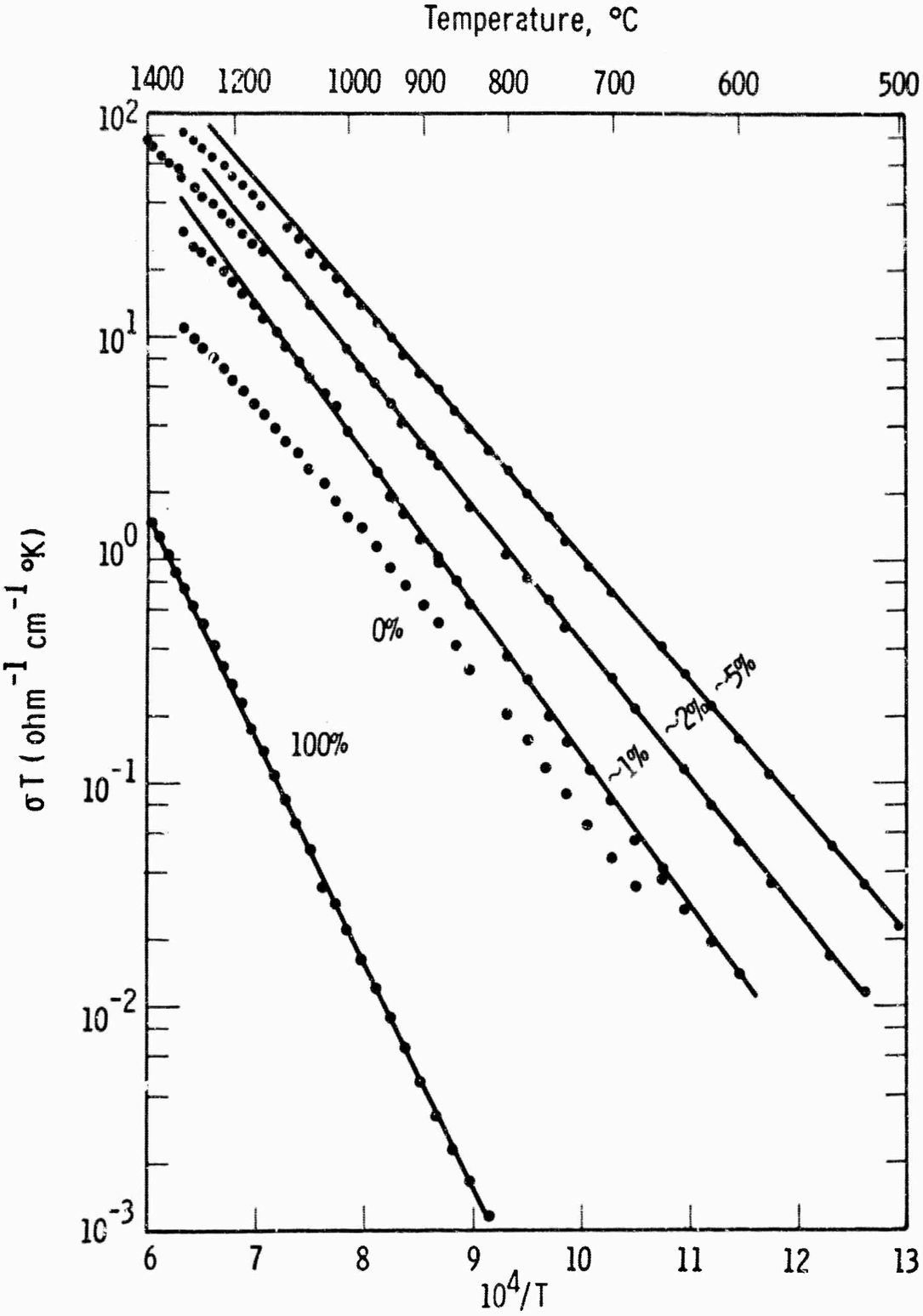

Fig. 6—Electrical conductivity of solid solutions of given mole % $YO_{1.5}$ in ThO_2

Scientific Paper 64-9F5-268-P1
Proprietary Class 3

July 29, 1964

HIGH TEMPERATURE INDUCTION FURNACE WITH OXIDE SUSCEPTORS

P.H. Sutter, E.C. Subbarao, and J. Hrizo

Abstract

Radio-frequency induction furnaces with refractory oxide susceptors operate at temperatures well above 2000°C in an air or oxygen atmosphere. The CaO-ZrO_2 susceptor furnace is easy to construct and is inexpensive if a relatively small 10 kilowatt, 4 megacycle rf generator is available.

BLANK PAGE

Scientific Paper 64-9F5-268-P1 July 29, 1964
Proprietary Class 3

HIGH TEMPERATURE INDUCTION FURNACE WITH OXIDE SUSCEPTORS

P.H. Sutter, E.C. Subbarao, and J. Hrizo

INTRODUCTION

The increased interest in high temperature materials has created numerous uses for very high temperature furnaces that can be operated in an oxidizing atmosphere rather than in a reducing atmosphere or vacuum. High temperature furnaces commonly use graphite or refractory metal heaters that require protection from oxygen. The type of furnace that is described here uses heaters and insulators that are stable in air at temperatures up to 2400°C. These furnaces have the additional advantages of being both easy to construct and inexpensive, if an appropriate radio-frequency generator is available.

The furnace consists simply of a stack of cylindrical oxide susceptor rings which conduct well enough at high temperatures to couple effectively with the radio frequency field of the work coil of the rf generator. The power dissipated in the susceptors is sufficient to heat the furnace to temperatures well over 2000°C. Since the electrical conductivity of the susceptor oxide, e.g. $CaO\text{-}ZrO_2$, is an exponentially rising function of the temperature, it is necessary to use some auxiliary method of preheating the susceptors until they couple sufficiently to the rf work coil to heat themselves to high temperature.

A furnace of this type has been described by Davenport et al.,[1] who inductively heated stabilized zirconia after preheating with powdered graphite in a 15 kw, 10 mc oscillator. A similar furnace was described by Leipold and Taylor,[2] who used a 30 kw, 7 mc generator and preheated with resistance heating using a separate power supply. The purpose of this paper is to describe some of the features of furnaces used in this laboratory and, in particular, to indicate the relatively modest power requirements that were found to be sufficient for a useful, easily constructed furnace.

FURNACE CONSTRUCTION

The furnace illustrated in Fig. 1 has been used routinely at temperatures up to 2300°C. It is extremely easy to construct and preheat. The susceptor rings are commercial calcia stabilized zirconia, that is, about 15 mole percent CaO in ZrO_2. The rings are made by cutting nominal 2 inch OD, 1-1/2 inch ID tubing into one inch lengths. Short lengths are used in order to make long cracks parallel to the axis less likely. The rings do crack in use due to thermal expansion stresses, but this does not prevent the furnace from working. Davenport et al.[1] attributed the continued high current flow to electron emission across the gaps. The 4-turn work coil of 3/8 inch copper tubing is close to the terminals of the 10 kilowatt, 4 megacycle radio frequency generator in order to reduce the lead inductance. This relatively small generator was found to be sufficient to heat the zirconia susceptors to their melting point. Thermal insulation is provided by unstabilized, i.e. "pure" zirconia, grain. The unstabilized

grain is a much poorer electrical conductor than is the stabilized susceptor material and hence the absorption of rf power in the insulation is minimized. This furnace is of convenient size for the work in this laboratory and is easier to preheat than are the larger furnaces that were described by Davenport et al.[1] and by Leipold and Taylor.[2] A furnace similar in size to the one described by Leipold and Taylor has also been constructed and used here. A working temperature of over 2300°C was achieved with only a 10 kilowatt, 4 megacycle generator compared to the 30 kw, 7 mc generator that was used before.

PREHEATING

The electrical conductivity in calcia stabilized zirconia is due to the migration of oxygen ion vacancies. This ionic conductivity increases rapidly with temperature with an activation energy of about 1.2 ev. The conductivity[3] at 600°C is about 3×10^{-4} $ohm^{-1}cm^{-1}$ which is much too low for effective heating in the 4 megacycle radio frequency field. The conductivity rises to about 0.04 $ohm^{-1}cm^{-1}$ at 1000°C, 0.2 $ohm^{-1}cm^{-1}$ at 1200°C and higher as the temperature rises. Hence the power absorption in the susceptor becomes greater as the temperature rises until, at very high conductivity, the penetration depth of the rf field in the susceptor becomes small enough to reduce the heating effectiveness. This condition apparently occurs at the highest temperatures in the furnaces used here. At room temperature, the susceptor conductivity is so low that no heating occurs in the rf field. Therefore it is necessary to initially raise the

susceptor temperature by some auxiliary means. The most convenient method found at this laboratory has been the insertion of a silicon carbide ("globar") rod into the furnace. For the furnace shown in Fig. 1, a one-inch diameter globar is heated inductively by the rf field until the furnace reaches a temperature of about 1300°C. The field is then momentarily turned off and the globar is simply pulled out of the top of the furnace. When the field is again turned on, the susceptors are able to absorb enough power to heat the furnace to the desired high temperature.

SPECIMEN SUPPORT

The specimen or a small crucible is supported in the hot zone of the furnace on top of the stabilized zirconia tube that is shown in Fig. 1. This tube is in turn supported by a stainless steel cylinder which slides through a bearing at the bottom of the furnace. The bearing guides the support tubes and also prevents a flow of air through the furnace which otherwise would act as a chimney. The support tubes are easily raised and lowered with a small jack which makes it possible to position the specimen in the hot zone as well as to slowly raise it into and lower it out of the hot zone. The crucible arrangement that is shown in Fig. 2 has been used to insure a particularly clean atmosphere for heat treating specimens of ThO_2. Oxygen gas enters through the thoria support tube and continually flushes out the atmosphere in the crucible that contains the specimens.

SUSCEPTOR MATERIALS

Calcia stabilized zirconia has been used because it is cheap and is commercially available. Leipold and Taylor[2] used yttria stabilized zirconia. This material does have a somewhat higher conductivity than does the calcia stabilized zirconia but there does not seem to be any need to go the extra expense of using it, since $CaO-ZrO_2$ is satisfactory. The maximum temperature of the furnace is limited by the melting point of the susceptors. Still higher temperatures could be achieved by the use of susceptors made out of thoria, containing about 5 mole percent yttria in order to improve the electrical conductivity. The conductivity of the thoria is not as high as that of the zirconia and no practical furnace has been developed yet to take advantage of the much higher melting point of thoria.

TEMPERATURE CONTROL

The furnace temperature can be read by sighting in through the top with an optical pyrometer. The temperature in the hot zone is found to be uniform within about $\pm 50^{\circ}C$ over the two-inch long hottest sections. Since the conductivity increases and therefore the power absorption increases as the temperature rises, this type of furnace would appear to be very unstable. Indeed, as the temperature increases it is necessary to reduce the generator plate voltage in order to keep the temperature from rising too rapidly. However, it has been found that it is fairly easy to

maintain a desired temperature by manua'. control. If desired, an electronic controller could be used to automatically control the temperature by adjusting the rf power level. A total raidation pyrometer would be a suitable sensor for this use.

References

1. W.H. Davenport, S.S. Kistler, W.W. Wheildon and O.J. Whittemore, Jr., J. Am. Ceram. Soc. 33, 333 (1950).

2. M.H. Leipold and J.L. Taylor, "Temperature, Its Measurement and Control in Science and Industry," Vol. 3, Pt. 2, American Institute of Physics, Reinhold (1962).

3. T.Y. Tien and E.C. Subbarao, J. Chem. Phys. 39, 1041 (1963).

Figure Captions

Fig. 1 Stabilized Zirconia Susceptor Furnace.

The one-inch long sections of commercial CaO-ZrO_2 tube act as susceptors (1) in the rf field of the 4-turn work coil (2). The stack of susceptors is supported on a stabilized zirconia tube (3) which rests on the platform (4) that holds the furnace. Thermal insulation is provided by the cover (5) and unstabilized zirconia grain (6) contained within the 4-inch diameter quartz tube (7). Specimen to be heated can be placed on top of a stabilized zirconia tube (8) that is supported by a stainless steel rod (9) which slides through the bearing (10). This specimen support structure is raised and lowered in the furnace with a laboratory jack.

Fig. 2 Chamber for Heating ThO_2 Specimens in Pure Oxygen.

All of the parts are made of ThO_2. Oxygen flows along the path shown by the dark arrow to continuously flush out the chamber atmosphere. Samples are placed on top of the small inverted crucible (1) and are covered by the larger outer crucible (2). Oxygen enters through the thoria tube (3) and setter plate (4).

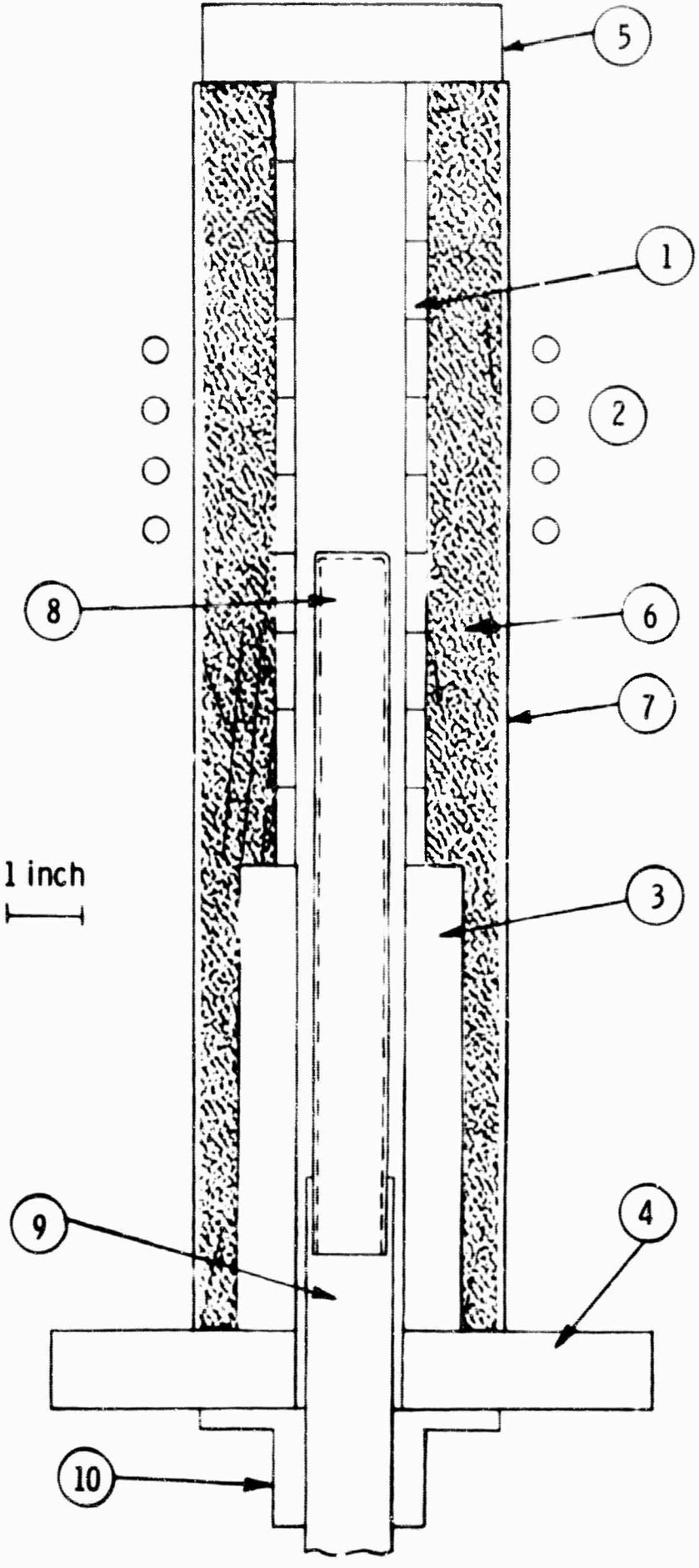

Fig. 1—Stabilized zirconia susceptor furnace

Dwg. 744A351

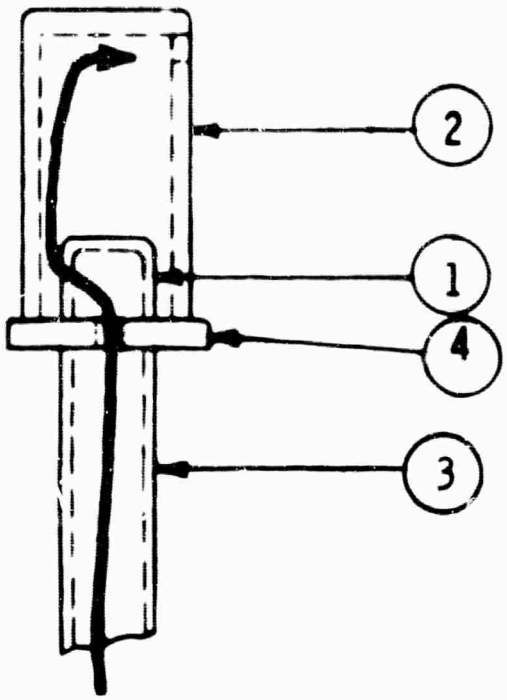

Fig. 2—Chamber for heating ThO_2 specimens in pure oxygen

DISTRIBUTION LIST

Atomic Energy Commission
Division of Research
Chemistry Programs
Washington 25, D. C. (1)

Atomic Energy Commission
Div. of Technical Information Extension
Post Office Box 62
Oak Ridge, Tennessee (1)

Commanding Officer
U.S. Army Chemical Research and
Development Laboratories
Edgewood Arsenal, Maryland
Attn: Librarian (1)

Dr. Galen R. Frysinger
Electric Power Branch
E.R.D.L.
Fort Belvoir, Virginia (1)

Director, ARPA
Attn: Dr. J. H. Huth
Material Sciences
Room 3D155, The Pentagon
Washington 25, D. C. (4)

Defense Contract Administrative
Service Region (P.T.)
401 Old Post Office Building
Pittsburgh 19, Pennsylvania
Attn: Mr. R. A. Mazula (1)

Defense Contract Administrative
Service Region (P.T.)
401 Old Post Office Building
Pittsburgh 19, Pennsylvania
Attn: Mr. T. J. Cortese (1)

Dr. A. W. Berger
TYCO, Incorporated
Bear Hill
Waltham, Massachusetts (1)

Dr. S. Schuldiner
Naval Research Laboratory, Code 6160
Washington 25, D. C. (1)

Mr. R. A. Osteryoung
Atomics International
Canoga Park, California (1)

Dr. David M. Mason
Stanford University
Stanford, California (1)

Dr. Howard L. Recht
Astropower, Inc.
2968 Randolph Avenue
Costa Mesa, California (1)

Mr. L. R. Griffith
California Research Corporation
576 Standard Avenue
Richmond, California (1)

Dr. Ralph G. Gentile
Monsanto Research Corporation
Boston Laboratories
Everett 49, Massachusetts (1)

Mr. Ray M. Hurd
Texas Research Associates
1701 Guadalupe Street
Austin 1, Texas (1)

Dr. C. E. Heath
Esso Research & Engineering Company
Box 51
Linden, New Jersey (1)

Dr. R. J. Flannery
American Oil Company
Whiting Laboratories
Post Office Box 431
Whiting, Indiana (1)

Aeronautical Systems Division
ASRMFP-2 (Mr. R. A. Garrett)
Wright-Patterson AFB, Ohio (1)

Dr. Douglas W. McKee
General Electric Company
Research Laboratories
Schenectady, New York (1)

DISTRIBUTION LIST

Commanding Officer
Office of Naval Research Branch Office
230 N. Michigan Avenue
Chicago 1, Illinois (1)

Commanding Officer
Office of Naval Research Branch Office
207 West 24th Street
New York 11, New York (1)

Commanding Officer
Office of Naval Research Branch Office
Box 39, Navy #100, F.P.O.
New York, New York (7)

Commanding Officer
Office of Naval Research Branch Office
1030 East Green Street
Pasadena 1, California (1)

Director, Naval Research Laboratory
Washington 25, D. C.
Attn: Technical Information Officer (6)
Chemistry Division (2)

Chief of Naval Research
Department of the Navy
Washington 25, D.C.
Attn: Code 425 (2)

DDR&E
Technical Library
Room 3C-128, The Pentagon
Washington 25, D. C. (1)

Department of the Army
Supply & Maintenance Command
Maintenance Readiness Division
Washington 25, D. C.
Attn: Technical Director (1)

U.S. Army Natick Laboratories
Clothing & Organic Materials Division
Natick, Massachusetts
Attn: Associate Director (1)

Harry Diamond Laboratories
Washington 25, D. C.
Attn: Library (1)

Office, Chief of Research & Development
Department of the Army
Washington 25. D. C.
Attn: Physical Sciences Div. (1)

Chief, Bureau of Ships
Department of the Navy
Washington 25, D. C.
Attn: Code 342A (2)

Technical Library, DLI-3
Bureau of Naval Weapons
Department of the Navy
Washington 25, D. C. (4)

Defense Documentation Center
Cameron Station
Alexandria, Virginia (20)

Commanding Officer
U.S. Army Electronic Research &
Development Laboratory
Attn: SELRA/DR
Fort Monmouth, New Jersey 07703 (1)

Naval Radiological Defense Laboratory
San Francisco 24, California, 94135
Attn: Technical Library (1)

Naval Ordnance Test Station
China Lake, California
Attn: Head, Chemistry Div. (1)

Commanding Officer
Army Research Office
Box CM, Duke Station
Durham, North Carolina
Attn: CRD-AA-IP (1)

REVISED 30 AUG 1963

DISTRIBUTION LIST

Dr. E. A. Oster
General Electric Company, DECO
Lynn, Massachusetts (1)

Prof. Herman P. Meissner
Massachusetts Institute of Technology
Cambridge 39, Massachusetts (1)

Dr. Paul Delahay
Department of Chemistry
Louisiana State University
Baton Rouge, Louisiana (1)

Mr. Donald P. Snowden
General Atomic
Post Office Box 608
San Diego 12, California (1)

Mr. C. Tobias
Chemistry Department
University of California
Berkeley, California (1)

Mr. Y. L. Sandler
Westinghouse Research Laboratories
Pittsburgh 35, Pennsylvania (1)

Dr. W. J. Hamer
Electrochemistry Section
National Science Foundation
Washington 25, D. C. (1)

Dr. Herbert Hunger
Power Sources Division
U.S. Army Signal Research and
Development Laboratory
Fort Monmouth, New Jersey (1)

Dr. T. P. Dirkse
Department of Chemistry
Calvin College
Grand Rapids, Michigan (1)

Dr. George J. Janz
Department of Chemistry
Rensselaer Polytechnic Institute
Troy, New York (1)

Mr. W. M. Lee, Director
Contract Research Department
Pennsalt Chemicals Corporation
900 First Avenue
King of Prussia, Pennsylvania (2)

Dr. B. R. Sundheim
Department of Chemistry
New York University
New York 3, New York (1)

Dr. E. M. Cohn
NASA
Code RPP
1512 H Street, N.W.
Washington 25, D. C. (1)

Dr. E. Yeager
Department of Chemistry
Western Reserve University
Cleveland 6, Ohio (1)

Lockheed Aircraft Corporation
Missiles and Space Division
Technical Information Center
3251 Hanover Street
Palo Alto, California (1)

Dr. A. B. Scott
Department of Chemistry
Oregon State University
Corvallis, Oregon (1)

Dr. V. I. Matkovich
The Carborundum Company
Niagara Falls, New York (1)

DISTRIBUTION LIST

Dr. A. M. Zwickel
Department of Chemistry
Clark University
Worcester, Massachusetts (1)

Arizona State University
Department of Chemistry
Dr. Michael O'Keeffe
Tempe, Arizona (1)

Dr. G. C. Szego
Institute for Defense Analysis
1666 Connecticut Avenue, N.W.
Washington 9, D. C. (1)

Mr. Horace W. Chandler
Assistant Manager
Research & Development Division
Isomet Corporation
433 Commercial Avenue
Palisades Park, New Jersey (1)

Mr. Neal P. Cockran, Chief
Division of Utilization
Office of Coal Research
Department of Interior
Washington 25, D. C. (1)

Naval Engineering Experiment Station
Annapolis, Maryland
Attn: Mr. J. H. Harrison (1)

Dr. R. F. Baddour
Department of Chemistry
Massachusetts Institute of Technology
Cambridge 39, Massachusetts (1)

CAPT G. E. Starkey
Aeronautical Systems Division
ASRMFP-2
Wright-Patterson AFB, Ohio (1)

Aerospace Corporation
P.O. Box 95085
Los Angeles 54, California
Attn: Technical Library
Documents Group (1)

Mr. T. W. Cushing, Manager
Military Service Department
Engelhard Industries, Inc.
113 Astor Street
Newark, New Jersey (1)

Thompson Ramo Wooldridge, nc.
23555 Euclid Avenue
Cleveland 17, Ohio
Attn: Mr. J. Ed Taylor
Associate Director, RD&E (1)

Engelhard Industries, Inc.
113 Astor Street
Newark 14, New Jersey (1)

Mr. N. F. Blackburn
E.R.D.L.
Materials Branch
Fort Belvoir, Virginia (1)